

國立交通大學

電機與控制工程學系

碩士論文

利用虛擬實境駕駛模擬進行雙重任務下分心之
腦波反應研究

**EEG Dynamics in Response to Distraction in
Virtual Reality Driving Simulation**

研究生：林弘章

指導教授：林進燈 博士

陳右穎 博士

中華民國 九十六 年七月

利用虛擬實境駕駛模擬進行雙重任務下分心效應之
腦波反應研究

**EEG Dynamics in Response to Distraction in Virtual Reality
Driving Simulation**

研 究 生：林弘章

Student : Hong-Zhang Lin

指導教授：林進燈 博士

Advisor : Dr. Chin-Teng Lin

陳右穎 博士

Dr. Yu-Ying Chen



A Thesis

Submitted to Department of Electrical and Control Engineering
College of Electrical and Computer Engineering
National Chiao Tung University
in Partial Fulfillment of the Requirements
for the Degree of Master
in
Electrical and Control Engineering
June 2007
Hsinchu, Taiwan, Republic of China

中華民國 九十六 年 七 月

利用虛擬實境駕駛模擬進行雙重任務下分心之 腦波反應研究

學生：林弘章

指導教授：林進燈 博士

陳右穎 博士

國立交通大學電機與控制工程研究所

中文摘要

駕駛者分心已經證實是造成車禍發生的重大原因之一。因此，本論文以腦電波(Electroencephalogram, EEG)來探討駕車行為下人類分心效應的腦部反應變化。研究中使用虛擬實境技術之動態駕車裝置，來模擬真實之駕車環境。在此實驗中，我們設計非預期性的車子偏移與數學問題的出現，來探討雙重任務所造成的分心效應。同時，為了進一步探討偏移和數學此二種任務在不同時間出現下的相互影響程度，我們設計了五個在事件出現時間點上有差異的狀況，並找出二種任務在不同的出現時間點，所造成腦電波上分心效應的反應變化。EEG 訊號經過獨立成份分析(Independent Component Analysis, ICA)後分離成數個獨立的訊號源，再利用事件相關頻譜擾動(Event Related Spectral Perturbation, ERSP)來計算事件發生前與後的頻譜變化，並經由此來觀察腦不活動在不同時間點上的頻譜差異。結果發現在額葉的區域，Theta 頻帶 (5~7.8 Hz) 和 Beta 頻帶 (12.2~17 Hz) 的能量會因為分心效應而增強。在枕葉區域，觀察到因為視覺刺激所誘發的反應現象以及因為回答數學問題按按鍵所產生的放鬆現象。在運動皮質區觀察到在 Alpha 頻帶因為事件誘發的能量抑制。以上所發現的腦部活化結

果在不同受測者均可以觀察到相同的反應。由以上這些結果我們能證明在駕駛事件與數學題目出現時間點有差異的狀況下，行為反應和腦波反應也相對應有變化。此一實驗結果也發現在額葉區域的 Theta 頻帶能量增強變化可以作為日後偵測駕駛者在實際駕駛中是否有分心的指標。

關鍵字：分心、雙重任務、腦電波、額葉、Theta 頻帶、數學、事件相關頻譜擾動、獨立成份分析



EEG Dynamics in Response to Distraction in Virtual Reality Driving Simulation

Student: Hong-Zhang Lin

Advisor: Dr. Chin-Teng Lin

Dr. Yu-Ying Chen

Department of Electrical and Control Engineering

National Chiao Tung University

Abstract

Driver distraction has been recognized as a significant cause of traffic incidents. Therefore, the aim of this study was to investigate Electroencephalography (EEG) dynamics in response to distraction during driving. To study human cognition under specific driving task, we used Virtual Reality (VR) based driving simulation to simulate events including unexpected car deviations and mathematics questions (math) in real driving. For further assessing effects of the stimulus onset asynchrony (SOA) between the deviation and math presented on the EEG dynamics, we designed five cases with different SOA. The scalp-recorded EEG channel signals were first separated into independent brain sources by Independent Component Analysis (ICA). Then, the Event-Related-Spectral-Perturbations (ERSP) measuring changes of EEG power spectra was used to evaluate the brain dynamics in time-frequency domains. Results showed that increases of theta band (5~7.8 Hz) and beta band (12.2~17 Hz) power were observed in the frontal cortex. For occipital components, we found the pattern of visual induced brain activities and rebounds from the button press. In motor components, we found alpha suppressions time-locked to event onsets. All the above results were consistently observed across 11 subjects. Results demonstrated that

reaction time and multiple cortical EEG sources responded to the driving deviations and math occurrences differentially in the stimulus onset asynchrony. Results also suggested that the phasic theta increase in frontal area could be used as the distracted indexes for early detecting driver's inattention in the real driving in the future.

Keyword: Distraction, Dual task, Frontal lobe, Theta band, Mathematics, Mental Workload, EEG, ICA, Component Clustering, ERSP, ERP.



誌 謝

本論文的完成，首先要感謝指導教授林進燈博士以及共同指導教授陳右穎博士這兩年來的悉心指導，讓我學習到許多寶貴的知識，在學業及研究方法上也受益良多。另外也要感謝口試委員們的建議與指教，使得本論文更為完整。

特別感謝美國加州聖地牙哥大學的 鐘子平教授、段正仁教授及 黃瑞松學長，給予我研究上最大的協助，從實驗設計、實驗分析、實驗結果討論到論文撰寫，給我最專業的意見跟看法。

另外，我要感謝腦科學研究實驗室的全體成員，沒有他們也就沒有我個人的成就。特別感謝 曲在雯博士、梁勝富教授、蕭富仁、林文杰教授給予我在各方面的指導，無論是研究上疑難的解答、研究方法、寫作方式、經驗分享等惠我良多。另外要感謝明達、仲良、俊傑、智文、德璋、林政同學，在過去兩年研究生生活中同甘共苦，相互扶持。此外，我也要感謝陳玉潔學姊、林君玲學姐、柯立偉學長、趙志峰學長、陳世安學長與黃騰毅學長在研究上的幫助，還有感謝德正、尚文、青甫、柏銓、玠瑤、孟修、依伶，在過去這一年中的相伴。同樣地也感謝實驗室助理 Amy、Apple、May 在許多事務上的幫忙。

謹以本文獻給我親愛的家人與親友們，以及關心我的師長，願你們共享這份榮耀與喜悅。

Contents

Contents	vii
List of Tables	x
List of Figures	xi
I. Introduction	1
II. Experimental Apparatus	5
2.1 Dynamic Driving Environment.....	6
2.2 EEG Signal Acquisition	9
2.3 3D Position Measurement of EEG Electrodes.....	11
2.4 Experimental Design.....	12
2.5 Subjects	16
III. Data Analysis	17
3.1 Analysis of the Behavior Data.....	17
3.2 The Procedures of EEG Data Analysis	19
3.3 Independent Component Analysis (ICA).....	20
3.4 Power Spectrum Analysis	23
3.5 Event Related Spectral Perturbation Analysis	24
3.6 Component Clustering	26
IV. Results	28
4.1 Behavior Performance	28
4.2 EEG Results of the Dual-Task Experiment	33
4.2.1 Distraction-Related Brain Sources.....	33
4.2.2 Event Related Spectral Perturbation Results in Single Subject.....	40
4.2.2.1 ERSP Results in Frontal Component.....	40
4.2.2.2 ERSP Results in Motor Component.....	43
4.2.2.3 ERSP Results in Parietal Component	46
4.2.2.4 ERSP Results in Occipital Component.....	47
4.2.3 Independent Component (IC) Clustering.....	48
4.2.3.1 Cross-Subject Power Spectra Results	50
4.2.3.2 Cross-Subject ERSP Results	54
V. Discussion	62
5.1 Brain Dynamics Related to Distracted Effect.....	62
5.1.1 Distracted Effect in Frontal Area	62

5.1.2 Distracted Effect in Mu Area	65
5.1.3 Distracted Effect in Occipital Area	66
5.2 Brain Dynamics Related to Dual Task.....	67
5.3 The Correlation between Behavioral and Physiological Responses.....	68
VI. Conclusions	70
Reference	72
Appendix.....	79
A. Independent Component Analysis (ICA).....	79



List of Tables

Table-1: The Specification of driving simulator	8
Table-2: Specifications of NuAmps	11
Table-3: The normalized response time to deviation and math	32
Table-4: The Number of Components in Different Clusters.....	50



List of Figures

Fig. 2-1: The illustration of the experimental setup including the dynamic VR driving environment and the EEG-based physiological measurement system.	5
Fig. 2-2: Pictures showed the dynamic VR driving environment, in the Brain Research Center of National Chiao Tung University, Taiwan, and ROC.....	7
Fig. 2-3: The picture showed the configuration of the 3D surrounded scene.....	8
Fig. 2-4: The picture showed the overview of surrounded VR scene.....	9
Fig. 2-5: Schematic pictures showed the lateral (A) and top view (B) of international 10-20 system of electrode placement [24].....	9
Fig. 2-6: The picture showed the setup of the physiological recording containing the NuAmps EEG amplifier and the electrode cap.....	10
Fig. 2-7: The picture showed the Fastrak 3D Digitizer.....	11
Fig. 2-8: The photomicrograph showed the simulated high way scene.....	12
Fig. 2-9: The illustration of the high way scene.....	13
Fig. 2-10: The illustration of the experimental paradigm.....	14
Fig. 2-11: The illustration of the deviation event.....	14
Fig. 2-12: The illustration of the relationship between the deviation onset and math occurred.....	15
Fig. 3-1: The flowchart of analyzing the behavioral data.....	18
Fig. 3-2: The flowchart showed the EEG signal processes.....	19
Fig. 3-3: The illustration of the ERP analysis.....	20
Fig. 3-4: Illustration of the concept of ICA process.....	21
Fig. 3-5: The picture showed the typical example of scalp topography of ICA decomposition.....	22
Fig. 3-6: The illustration of procedures in ERSP analysis.....	25
Fig. 3-7: The flowchart of component clustering by using K-means algorithm.....	27
Figure 3-8: The typical example of the component clustering result.....	27
Fig. 4-1: Bar charts of the averaged response time to the deviation (A) or the math (B) onsets between four cases.....	29
Fig. 4-2: Bar charts of normalized response time to the deviation (A) and math (B) presented between 5 cases across 11 subjects.....	31
Fig. 4-3: Scalp map topographies of ICA decomposition of subject-4.....	33
Fig. 4-4: The illustration of the component maps and their corresponded dipole locations.....	34
Fig. 4-5: Illustration of the typical example of six ICs and their power spectra from five different cases.....	36

Fig. 4-6: Single subject data. The comparison of total power spectra between single- and dual-task in the central midline component.	37
Fig. 4-7: Single subject data. The comparison of power spectral baselines between single- and dual-task cases in the motor component.	38
Fig. 4-8: Single subject data. The comparison of power spectra between single- and dual-task cases in the parietal component.....	38
Fig. 4-9: Single subject data. The comparison of power spectra between single- and dual-task cases in the frontal component.	39
Fig. 4-10: Single subject data. The ERSP plots of the single-task cases in the frontal component.....	41
Fig. 4-11: Single subject data. The ERSP plots of the dual-task cases in the frontal component.....	42
Fig. 4-12: Single subject data. The ERSP plots of the five cases in the frontal component.....	43
Fig. 4-13: Single subject data. The ERSP plots of the single-task cases in the motor component.....	44
Fig. 4-14: Single subject data. The ERSP plots of the five cases in the motor component ($p < 0.05$).....	45
Fig. 4-15: Single subject data. The ERSP plots of the five cases in the parietal component ($p < 0.05$).....	46
Fig. 4-16: Single subject data. The ERSP plots of the five cases in the occipital component ($p < 0.05$).....	48
Fig. 4-17: The scalp maps.....	49
Fig. 4-18: The grand mean of total power spectra for epochs from five cases in the frontal cluster across 10 subjects.	51
Fig. 4-19: The comparison of the averaged power around the 5~7.8 Hz and 12.2~17 Hz between the single task and dual tasks across 10 subjects in the frontal component.....	52
Fig. 4-20: The grand mean of the total power spectra for epochs from five different cases in the right motor cluster across 6 subjects.	53
Fig. 4-21: The comparison of the averaged alpha power between the single tasks and dual tasks in the motor cluster.....	54
Fig. 4-22: The ERSP images of frontal cluster for five cases.....	55
Fig. 4-23: The comparison of total power in cross-subject averaged ERSP images in frontal component between cases.	56
Fig. 4-24: Effects of distraction on onsets of theta and beta increases.	57
Fig. 4-25: The grand mean of cross-subject averaged ERSP images	57
Fig. 4-26: The comparison of total power in cross-subject averaged ERSP images ...	58

Fig. 4-27: The distracted effects on latencies of alpha suppression measured averaged ERSP images of the motor components.....59

Fig. 4-28: The grand mean of averaged ERSP images59

Fig. 4-29: The averaged ERPs of the left (left block: 7 subjects) and right (right block: 5 subjects) occipital clusters for five cases.60

Figure 5-1: Picture showed the principle fissures and lobes cerebrum63



I. Introduction

Distraction and inattention of drivers have been identified as the main leading causes of car accidents. The U.S. National Highway Traffic Safety Administration has identified driver distraction as a high priority area about 30% [1]. Driver distraction by whatever cause is a significant contributor to road traffic accidents [2] [3]. Driving is a complex task in which several skills and abilities are involved simultaneously. Monitoring drivers' attention related brain resources is still a challenge for researchers and practitioners in the field of cognitive brain research and human-machine interaction.

Reasons of distractions found during driving were quite widespread, including eating, drinking, talking with passengers, use of cell phones, reading, fatigue, problem-solving, and using in-car equipment. Recently, commercial vehicle operators with complex in-car technologies (such as navigation, road traffic information, mobile telephones and in-vehicle entertainment systems) are also at increased risk since drivers may become increasingly distracted in the years to come, thus making it likely that the problem of driver inattention [4] [5]. Some literatures studied the behavioral effect of driver's distraction in car. Tijerina's study was based on measurement of the static completion time of an in-vehicle task [6]. Similarly, the distraction effect caused by cellular phones during driving has been a focal point of recent in-car applications [7] [8] [9]. Experimental studies have been conducted to assess the impact of specific types of driver distraction on driving performance. While these studies have generally reported significant driving impairment [10] [11], simulator studies cannot provide information about the impact of these decrements on the occurrence of crashes

resulting in hospital attendance by the driver. Therefore, in order to provide information before the occurrence of crashes we try to investigate the drivers' physiological responses.

To the aspect of neural physiological investigation, some literatures focused on the brain activities of "divided attention" referring to attention divided between two or more sources of information, such as visual, auditory, shape, and color stimuli. Madden et al. [12] investigated brain activation when subjects were instructed to divide their attention among the display positions within the visual modality. Regional cerebral blood flow (rCBF) activation was found in occipitotemporal, occipitoparietal, and prefrontal regions. And Positron emission tomography (PET) measurements were taken while subjects discriminated between shape, color, and speed of a visual stimulus under conditions of selective and divided attention. The divided condition activated the anterior cingulate and prefrontal cortex in the right hemisphere [13]. In another study, functional magnetic resonance imaging (fMRI) was used to investigate the brain activity during a dual-task (visual stimulus) experiment. This found activation in the posterior dorsolateral prefrontal cortex and lateral parietal cortex [14]. Similarly, the study used electroencephalogram (EEG) to investigate mental arithmetic-induced workload increasing, the finding is power increase in theta band in the region of frontal lobes [15]. And, several neuroimaging studies showed the importance of the prefrontal network in dual-task management [16] [17]. However, the above-mentioned studies just investigated the brain activity of dual-task interaction without considering the stimulus onset asynchrony (SOA) problem during driving and the effect of different temporal relationship of stimuli.

The current investigation utilized an array of methodological assessment techniques and compared the sensitivity of each to changes in attention processing requirements as a function of driving task demand. Some literatures of investigated

the traffic record the electroencephalogram (EEG) to compare the P300 amplitude [18]. During simulated traffic scenarios, resource allocation was assessed through as event-related potential (ERP) novelty oddball paradigm [19]. However, these are just to analyze in time course, we can take one step to analyze the relation between time and frequency course.

The electroencephalogram (EEG) has been used for 80 years in clinical practices as well as basic scientific studies. Nowadays, EEG measurement is widely used as a standard procedure in researches such as sleep studies [20], epileptic abnormalities, and other disorders diagnoses. Comparing to another widely used neuroimaging modality, functional Magnetic Resonance Imaging (fMRI), EEG is much less expensive and has the superior ability of temporal resolution for us to investigate the SOA problems. Furthermore, to avoid the interference and risks of operating an actual vehicle on the road, the use of driving simulation for vehicle design and studies of driver's behavior and cognitive states is also expanding rapidly [21] [22]. The static driving simulation may be difficult to approach the realistic driving condition, such as the vibrations that would be experienced when driving an actual vehicle on the road. The VR technique allows subjects to interact directly with a virtual environment rather than monotonic auditory and visual stimuli. Integrating realistic VR scenes with visual stimulus is easier to study the brain response to visual attention during driving. Therefore, in recent years, the VR-based simulation combined with electroencephalogram (EEG) monitoring is an innovation in cognitive engineering research [20] [23].

The main goal of this study is to investigate the brain dynamics related to distraction by using EEG and VR-based realistic driving environment. Unlike the previous studies, our experiment has three main characteristics. First, the stimulus onset asynchrony (SOA) experimental design, the different appearance time of dual

tasks (mathematical questions and unexpected car deviation), has the benefits for us to investigate the driver's behavioral and physiological response under multiple conditions and multiple distracted levels. Second, the ICA-based advanced signal analysis methods were used to extract the artifact-free brain responses and related cortical location related to the single/dual task. Third, compared with single task, the interaction and effect of dual-task-related brain activities was also investigated. The detailed contents are described in the following sections.

The thesis was organized in 6 chapters. Chapter 1 briefly introduced current knowledge in vestibular system and the goal of the study. Chapter 2 detailed the apparatus and materials of the study. Chapter 2 also described the details of experimental setup, including the time course of event onset asynchrony setup. In chapter 3, we explored the EEG with innovative methods by combining Independent Component Analysis (ICA), time-frequency spectral analysis, power spectrum and component clustering. Chapter 4 showed the results. Chapter 5 discussed and compared our finding with previous studies, and finally we concluded in Chapter 6.

II. Experimental Apparatus

The main purpose of this research was to investigate the EEG features related to distraction in a dual-task experiment. The most concerned issue in dual-task studies was the effect of distraction on driving because it directly related to public safety. For example, using cell-phone, tuning radio or looking at the road-sign could distract the drivers from their driving task and cause serious traffic accidents. However, the driving experiments were very dangerous if they were took place on road. With combining the technology of virtual reality (VR), a driving environment was constructed for the safety of driving experiments in our lab. The VR-based dynamic environment could provide realistic visual and motion stimuli to the subjects. The environment was employed in the setup of dual-task experiment as shown in Fig. 2-1.



Fig. 2-1: The illustration of the experimental setup including the dynamic VR driving environment and the EEG-based physiological measurement system.

There were three major parts of the architecture: (1) a 3D highway driving scene based on the VR technology, (2) a real vehicle mounted on a 6-DOF motion platform, (3) a physiological signal measurement system with 36-channel EEG/EOG/ECG sensors. The subjects were asked to sit in a real car mounted on the 6-DOF motion platform with their hands holding the steering wheel to control the simulated car in the VR scene. The 30-channel scalp EEG and 4-channel EOG were simultaneously recorded at 1 KHz sampling rate. The details of the experimental setup would be presented in the following sections.

2.1 Dynamic Driving Environment

A virtual-reality (VR) based highway-driving environment was used to investigate the changes on drivers' distraction effect. The VR driving environment includes 3D surround scenes projected by seven projectors and a real car mounted on a 6-degree-of-freedom (as showed in Fig. 2-2) Stewart platform to provide the kinesthetic stimuli. The dynamic driving environment provided a safe, time saving and low cost approach to study human cognition under realistic driving events. The subjects could interact directly with the environment and receive the most realistic driving conditions during the experiments.



Fig. 2-2: Pictures showed the dynamic VR driving environment, in the Brain Research Center of National Chiao Tung University, Taiwan, and ROC. A real car in the 3D VR environment was showed in the left picture. The experimental setup around the steering wheel was showed in the right picture.

In this study, the VR scene was generated by the Virtual- Reality technology with a World Tool Kit (WTK) library. The C program including the WTK library was used and its library function was called up to move the three-dimensional models. The 3D view was composed of seven identical PCs running the same VR program. Seven PCs were synchronized by LAN so all scenes were going at exactly same pace. The VR scenes of different viewpoints were projected on corresponding locations. Fig. 2-3 showed the layout of our simulator. The front screen marked 1 and 2 was overlapped by two polarized frames to reach the binocular parallax. The frames for the left and right eyes were projected onto the frontal screen with two projectors, respectively. By wearing special glasses with a polarized filter, the configuration provided a stereoscopic VR scene for a 3D visualization. In our VR scene, the surrounded screens covered 206° frontal FOV and 40° back FOV, as shown in Fig. 2-4. Frames projected from 7 projectors were connected side by side to construct a surrounded VR scene. The size of each screen had diagonal measuring 2.6-3.75 meters. The vehicle was placed at the center of the surrounded screens. Detailed information was shown in Table-1.

Table-1: The Specification of driving simulator

Screen Number or Location	Dimension
Screen Number 1, 2, 3, 4 (FOV 42°)	(W)×(H) = (300 cm)×(225 cm)
Screen Number 5, 6 (FOV 40°)	(W)×(H) = (270 cm)×(202 cm)
Screen Number 7 (FOV 40°)	(W)×(H) = (210 cm)×(157 cm)
Vehicle Dimension	(L)×(W)×(H) = (430 cm)×(155 cm)×(140 cm)
Driver to Front Screen (1, 2)	370 cm
Driver to Left and Right Screen (5, 6)	220 cm (Left) and 300 cm (Right)
Driver Head Height Relate to Screen 1	120 cm



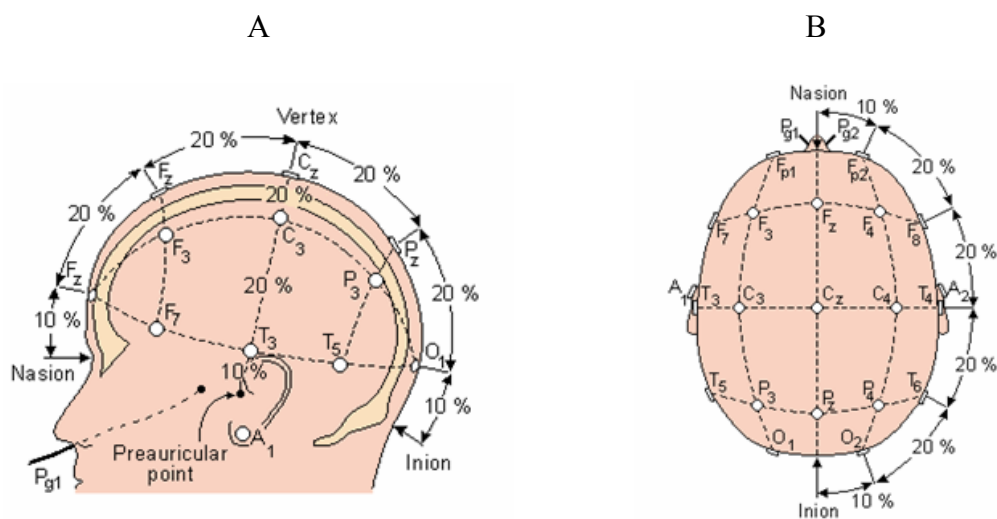
Fig. 2-3: The picture showed the configuration of the 3D surrounded scene. The 3D VR scene consisted of 7 projectors, creating a surrounded view. The frontal screen was overlapped by 2 projector frames in different polarizations, providing a stereoscopic VR scene for 3D visualization.



Fig. 2-4: The picture showed the overview of surrounded VR scene. The VR-based four-lane highway scenes were projected into surround screen by seven projectors.

2.2 EEG Signal Acquisition

An electrode cap was mounted on the subject's head for signal acquisition as shown in Fig. 2-5. A standard for the placement of EEG electrodes proposed by Jasper in 1958, which is known as the 10-20 International System of Electrode Placement [24] is used in the electrode cap. An illustration of the 10-20 system is shown in Fig. 2-5, the electrodes are named according to the location of an electrode and the underlying area of cerebral cortex.



The letters F, C, T, P, and O were refer to the frontal, central, temporal, parietal, and occipital cortical regions on the scalp, respectively. The term “10-20” means 10% and 20% of the total distance between specified skull locations. The percentage-based system allowed differences in skull locations. The physiological data acquisition used 30 sintered Ag/AgCl EEG/EOG electrodes with a unipolar reference at right earlobe and 2 ECG channels in bipolar connection placed on the chest.

The 36 electrodes including 34 EEG/EOG channels , 2 ECG channels (bipolar connections between the right clavicle and left rib), and one 8-bit digital signal produced form VR scene were simultaneously recorded by the Scan NuAmps Express system (Compumedics Ltd., VIC, Australia) shown in Fig. 2-6. It was a high-quality 40-channel digital EEG amplifier capable of 32-bit precision sampled at 1000 Hz. Table-2 showed the specifications of the NuAmps amplifier. Before acquiring EEG data, the contact impedance between EEG electrodes and skin was calibrated to be less than 5k Ω by injecting NaCl based conductive gel. The EEG data were recorded with 16-bit quantization levels at a sampling rate of 500 Hz in this study. All EEG data were preprocessed using a low-pass filter with a cut-off frequency of 50 Hz in order to remove the power line noise and other high-frequency noise. Similarly, a high-pass filter with a cut-off frequency at 0.5 Hz was applied to remove baseline drifts.



Fig. 2-6: The picture showed the setup of the physiological recording containing the NuAmps EEG amplifier and the electrode cap.

Table-2: Specifications of NuAmps

Analog inputs	40 unipolar (bipolar derivations can be computed)
Sampling frequencies	125, 250, 500, 1000 Hz per channel
Input Range	$\pm 130\text{mV}$
Input Impedance	Not less than 80 MOhm
Input noise	1 μV RMS (6 μV peak-to-peak)

2.3 3D Position Measurement of EEG Electrodes

The Fastrak 3D Digitizer is an accurate electromagnetic tracking system we used for localization of electrodes. With the 3D digitizer, it became possible to construct accurate anatomical/functional images from the surface measured potentials. Fastrak is controlled by software named Locator, which acquires and displays 3D position measurements for electrodes. It includes a System Electronics Unit (SEU), a power supply, three cube receivers, one stylus and one standard transmitter (as showed in Fig. 2-7). Used the hardware and software necessary to generate and sense the magnetic fields, compute position and orientation for digitizing electrode locations of subject's head.

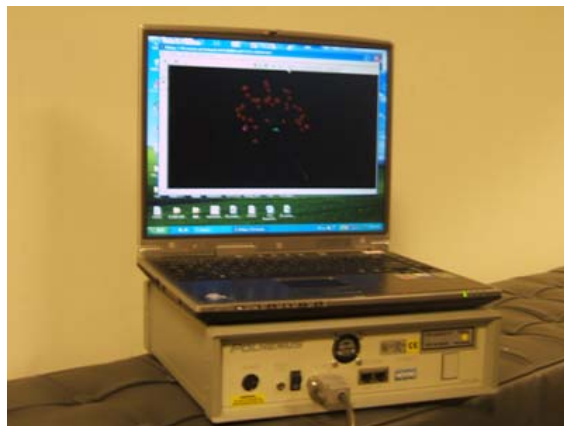


Fig. 2-7: The picture showed the Fastrak 3D Digitizer.

2.4 Experimental Design

To investigate the effect of stimulus onset asynchrony (SOA) on the behavioral performance and differences on brain activities between single- and dual- task condition in a virtual environment, we designed two tasks: unexpected car deviation, mathematical questions. We used the combinations of these two tasks to provide different distracted effects to the subjects.

We developed a VR highway environment with a monotonic scene as shown in Fig. 2-8 and eliminated all unnecessary visual stimuli. The four lanes from left to right were separated by a median strip in the VR-based scene. The distance from the left side to the right side of the road was equally divided into 256 points for outputting digital signal from WTK program, and the width of each lane and the car was 60 units and 30 units, respectively (as showed in Fig. 2-9). In the VR scene, the simulated driving speed was controlled by a scheduled program, thus subjects need not to step on paddles, to prevent large muscle activity on the throttle or brake.



Fig. 2-8: The photomicrograph showed the simulated high way scene. The monotonous scene was designed to reduce the visual disturbance.

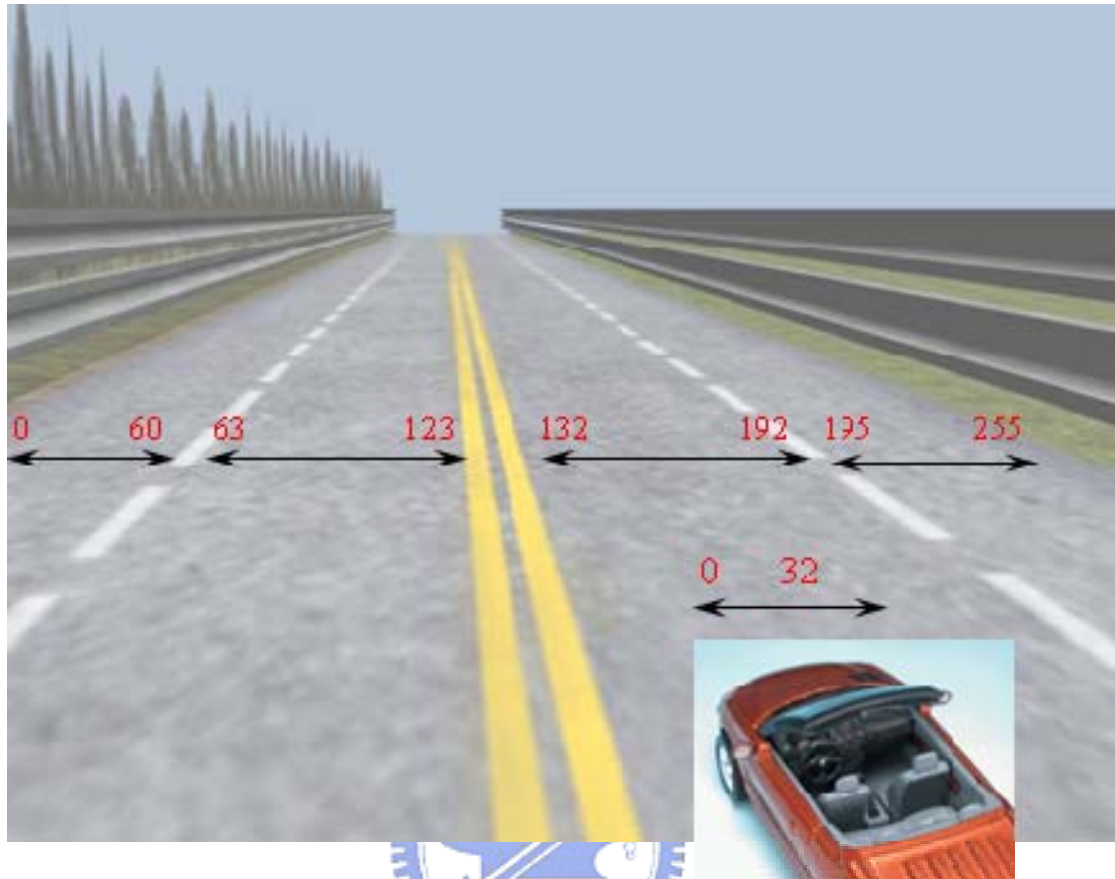


Fig. 2-9: The illustration of the high way scene. The width of highway from the left to right side was equally divided into 256 units and the width of the car was 32 units.

There would be four 15-minute sessions (5~10 minutes break between sessions to avoid the subject get drowsy) in one driving simulation experiment for each subject. To avoid anticipative effect for subjects the events were presented to the subjects randomly, as shown in Fig. 2-10. The inter-trial intervals were set from 6 to 8 seconds in order to avoid interaction between trial and trial. Thus a total of 100 events could be presented to the subject in each session to ensure the number of events is enough for statistical analysis.

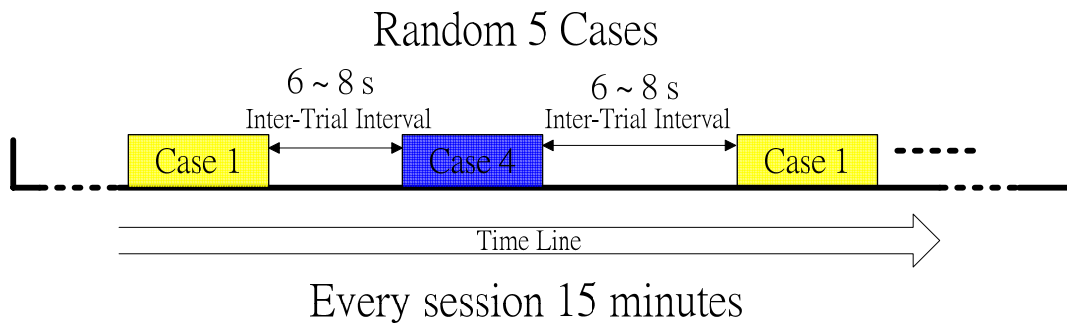


Fig. 2-10: The illustration of the experimental paradigm. Five cases were randomly appeared and the inter-trial intervals were varied from six to eight seconds. There were four sessions (15 minutes / per session) in each experiment.

Since the main purpose of this experiment was to investigate the distracted effect in dual-task conditions. Therefore, two driving tasks were designed including the car unexpected deviation and the mathematical questions. The car would randomly drift from the middle of the road in a deviation task. When the event was occurred, subjects had to control the steering wheel to keep car in the third lane (as showed in Fig. 2-11).

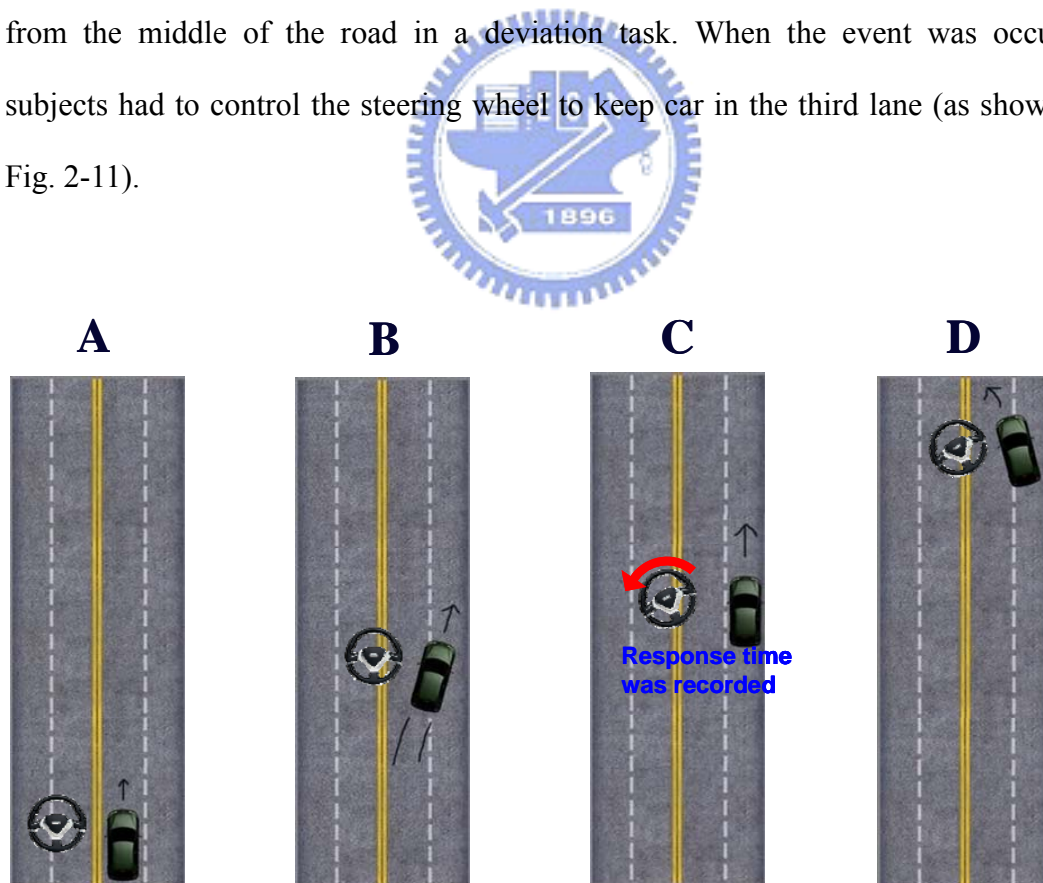


Fig. 2-11: The illustration of the deviation event. (A) Vehicle moving in straight line; (B) the onset of deviation event; (C) response to the deviation and (D) vehicle back to middle lane.

Two digits addition equations were presented to the subjects in the mathematics task. The answers of the equations were already designed to present with the equations but they could be either right or wrong. The subjects were asked to press the right bottom on the steering wheel when the equation is correct, and to press the left bottom when it was wrong. The event allotment ratios were 50% and 50% for right and wrong equations, respectively.

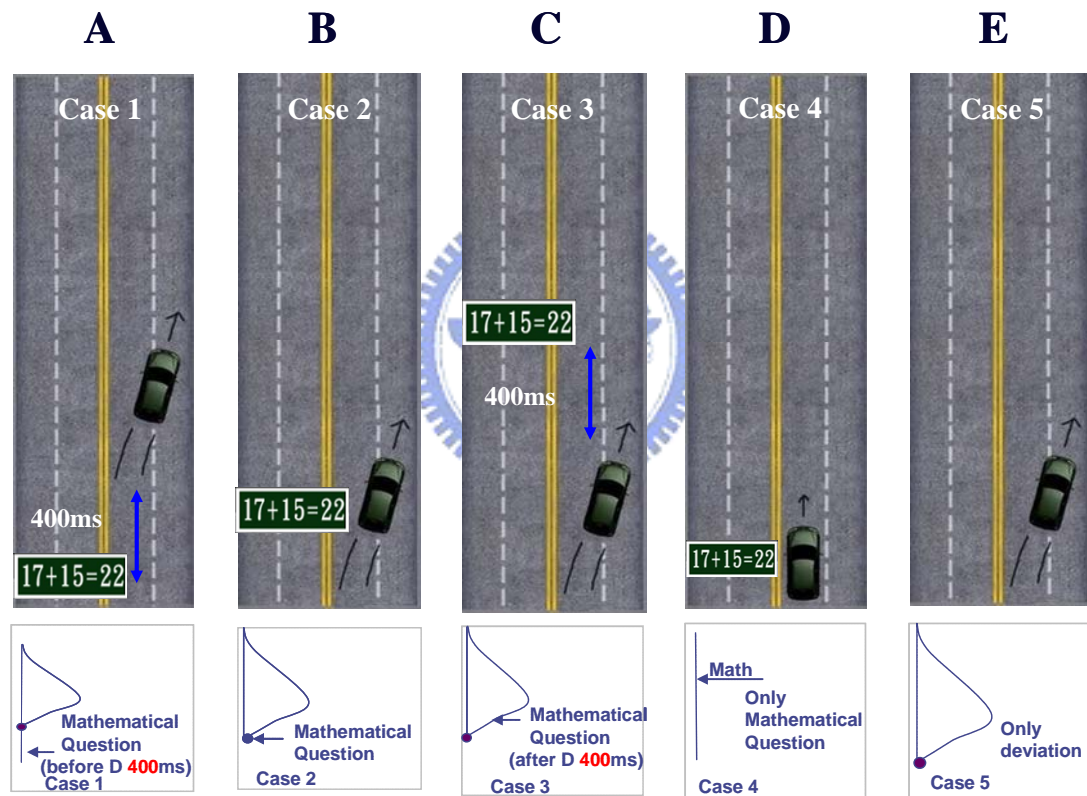


Fig. 2-12: The illustration of the relationship between the deviation onset and math occurred. (A) Case 1: math was presented at 400ms before the deviation onset. (B) Case 2: math and deviation occurred at the same time. (C) Case 3: math presented at 400ms after the deviation onset. (D) Case 4: only math presented. (E) Case 5: only deviation occurred.

The combinations of these two tasks were used to provide different distracted conditions to the subjects. Five conditions were developed to study the interaction of

the two tasks, they are: (A) math was presented at 400ms before deviation (math-400ms-deviaiton), (B) two tasks were presented at the same time (math-deviation) (C) math was presented at 400ms after deviation (deviation-400ms-math), (D) only math presented (single-math) and (E) only deviation occurred (single-deviation). The illustrations of the five conditions were shown in Fig. 2-12. A pilot study was designed to determine the time of stimulus onset asynchrony, i.e., the time interval between two tasks in case 1 and 3. Three different time values were tested including 400ms, 800ms and 1200ms. The behavioral data was collected from 8 subjects in the pilot study. The result suggested the interaction between tasks is significant with 400ms time interval. Thus, we adopted 400ms as the time of stimulus onset asynchrony.

2.5 Subjects



Eleven healthy volunteers (all males) with no history of gastrointestinal, cardiovascular, or vestibular disorders participated in the experiment of the motion-sickness study. The subjects are ages from 20 to 28 years old, with a mean of 24 years. They were requested not to smoke, drink caffeine, use drugs, or drink alcohol, all of which could influence the central and autonomic nervous system for a week prior to the main experiment.

III. Data Analysis

After the recording of the multi-channel EEG signals and behavior data, the data were analyzed for the study of distracted effect. The software of Statistical Package for Social Science (SPSS) was used to estimate the significant testing of behavior data. EEG epochs were extracted from the recorded EEG signals after down sampling, filter and artifact removal. We used Independent Component Analysis (ICA) [25] to separate independent brain sources. The Event Related Potential (ERP) was first used to study the EEG potential responses in time domain. The Event Related Spectral Perturbation (ERSP) technology was then applied to the ICA component signals to transfer the signal into time-frequency domain for the event-related frequency study. The stability of component activations and scalp topographies of meaningful components were finally investigated with component clustering technology.



3.1 Analysis of the Behavior Data

The response time of the tasks (the deviation and the math) was analyzed to study the behavior of the subjects in the experiments. By using one way analysis of variance (ANOVA), the significance of the behavior data were tested for every subject and the nonparametric test to study the trend of the behavior data. Fig. 3-1 showed the flowchart of analysis behavior data. First, we had to remove the outliers by using the criterion of $\text{mean} \pm 3D$ (mean: average the response time, D: standard deviation). Then we choose the minimal trial in all cases to make benchmark. And we used the benchmark to select randomly the same trials in other cases. Single task was baseline, and choose the minimal value as denominator. To normalize the behavior data was [Xi

$\div(X_{\text{mean}})]$ (X_i : Every response time of trial, X_{mean} : mean response time in single case). Because several extremely large scores significantly skewed, so nonparametric analysis was used. A Friedman ANOVA was conducted to test for difference in R-values ($X_i \div (X_{\text{mean}})$) among the five in-vehicle tasks.

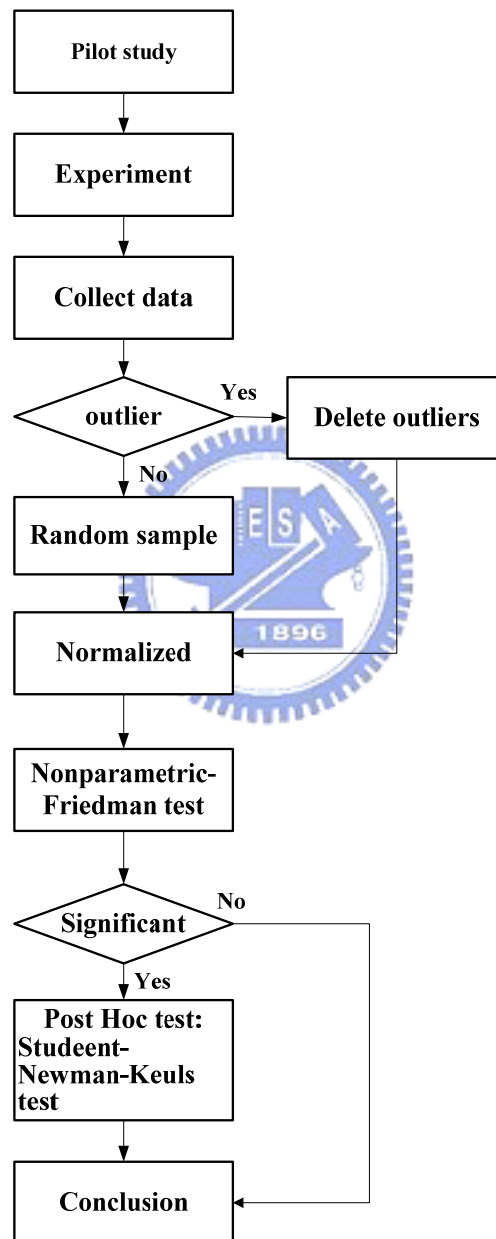


Fig. 3-1: The flowchart of analyzing the behavioral data. First, we removed the outliers and normalized the behavioral data by $[X_i \div (X_{\text{mean}})]$ (X_i : Every response time of trial, X_{mean} : mean response time in single case) and then we used the Friedman test to examine the significance of R-values ($X_i \div (X_{\text{mean}})$). Finally, the Student-Newman-Keuls test was used to assess the significant within all cases.

3.2 The Procedures of EEG Data Analysis

Fig. 3-2 showed the flowchart of the proposed data analysis procedure for EEG signals. The EEG data were recorded with 16-bit quantization level at a sampling rate of 500 Hz and the recording were down-sampled to sampling rate (SR) =250 Hz for the simplicity of data processing. The EEG data were then preprocessed using a simple low-pass filter with a cut-off frequency of 50 Hz to remove the line noise (60 Hz and its harmonic) and other high-frequency noise for further analysis. A simple high-pass filter with a cut-off frequency of 0.5 Hz was used to remove the DC drift. Then we extracted epochs from continuous EEG data and combine all epochs to run independent component analysis (ICA). Finally, we applied the technology of Event-Related-Spectral-Perturbations (ERSPs) to investigate the EEG responses in both time and frequency domains.

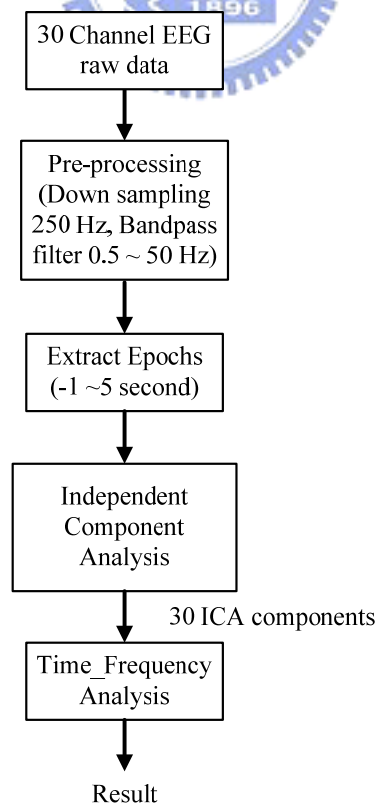


Fig. 3-2: The flowchart showed the EEG signal processes.

Since we had designed different cases with the combinations of the driving and the mathematic tasks, thus the EEG response related to different cases should be extracted from the original EEG signals for further analysis. The event-related potentials (ERPs) were extracted from the EEG signal as shown in Fig. 3-3.

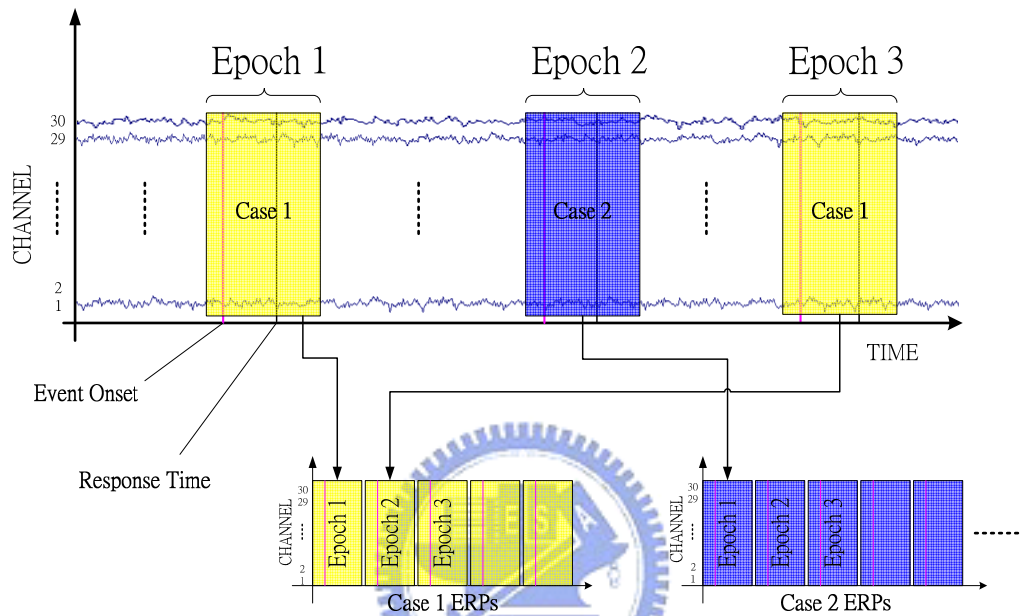


Fig. 3-3: The illustration of the ERP analysis. The case-related ERPs were extracted from raw EEG signals. Each epoch was extracted with the duration of 1 second before and five seconds after first event onset. The onset of first event was the occurrence of either the math or the deviation event depended on the case was presented.

3.3 Independent Component Analysis (ICA)

In order to extract the electroencephalographic (EEG) source segregation, identification, and localization were very difficult. Because the EEG data collected from any point on human scalp induces activity generated within a large brain area. Although the conductivity between the skull and brain was different, the spatial smearing of EEG data by volume conduction did not cause significant time delay and

it suggests that the ICA algorithm is suitable for performing blind source separation on EEG data. The ICA methods were extensively applied to blind source separation problem since 1990s [26]-[33]. The reports of study [34]-[41] demonstrated that ICA was a suitable solution to solve the problem of EEG source separation, identification, and localization. They assumed that: (a) the conduction of the EEG sensors is instantaneous and linear such that the measured mixing signals are linear and the propagation delays are negligible. (b) The signal source of muscle activity, eye, and cardiac signals are not time locked to the sources of EEG activity which is regarded as reflecting synaptic activity of cortical neurons.

$$\mathbf{x}(t) = \mathbf{A}\mathbf{s}(t) \quad (1)$$

Where \mathbf{A} is a linear transform called a mixing matrix and the s_i are statistically mutually independent. The ICA model estimates a linear mapping \mathbf{W} such that the unmixed signals $\mathbf{u}(t)$ are statically independent (as showed in Fig. 3-4) (The detail was in Appendix).

$$\mathbf{u}(t) = \mathbf{W}\mathbf{x}(t). \quad (2)$$

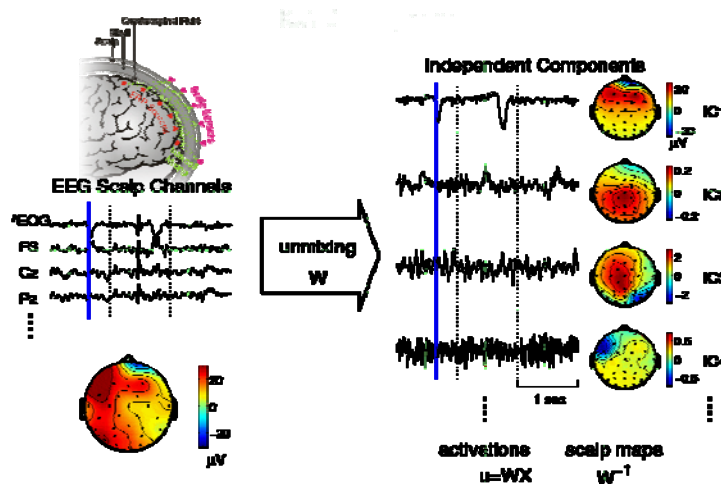


Fig. 3-4: Illustration of the concept of ICA process. EEG signals recorded from the brain were mixed with multiple sources [62]. By training the unmixing matrix, the mixed EEG signals were separated into independent components which may have specific meanings, and then scalp maps was plotted according to the weight of unmixing matrix.

In this study, we attempted to completely separate the twin problems of source identification and source localization by using a generally applicable ICA. Thus, the artifacts including the eye-movement (EOG), eye-blinking, heart-beating (EKG), muscle-movement (EMG), and line noises can be successfully separated from EEG activities. Fig. 3-5 showed a result of the scalp topographies of ICA weighting matrix W corresponding to each ICA component by projecting each component onto the surface of the scalp, which provided evidence for the components' physiological origins, e.g., eye activity was projected mainly to frontal sites, and the drowsiness-related potential was on the parietal lobe and occipital lobe [20], motor related potential will locate at left and right side of front parietal lobe, etc. We could see that most of artifacts and channel noises were effectively separated into independent components 1 and 20.

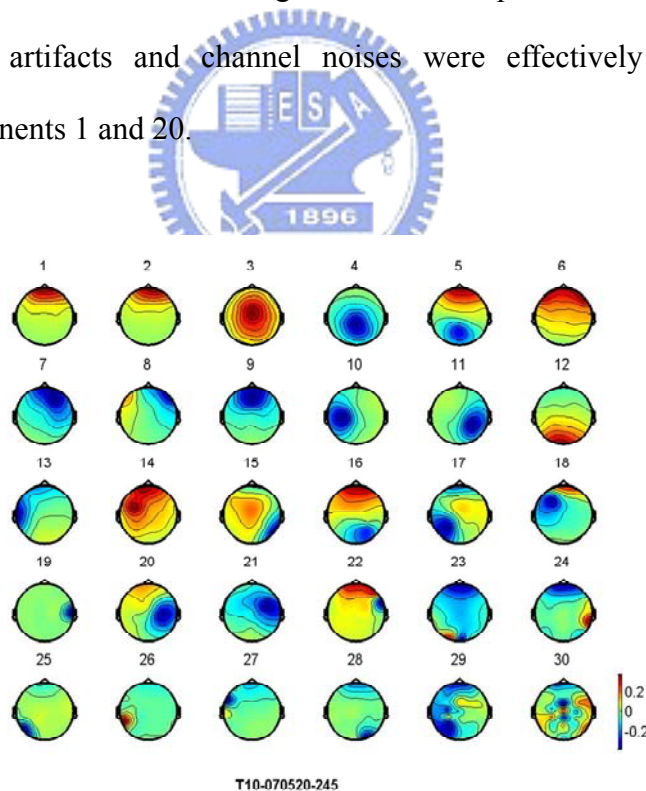


Fig. 3-5: The picture showed the typical example of scalp topography of ICA decomposition. The scalp topographies showed the ICA weighting matrix W projected to its corresponded component onto the surface of the scalp. The color bar was the amplitude of component signals.

3.4 Power Spectrum Analysis

Analysis of changes in spectral power and phase can characterize the perturbations in the oscillatory dynamics of ongoing EEG. Applying such measures to the activity time courses of separated independent component sources can avoid the confounds caused by misallocation of positive and negative potentials from different sources to the recording electrodes, and by misallocation to the recording electrodes activity that originates in various and commonly distant cortical sources. The spectral analysis for each ICA component decomposed from 30 channels of the EEG signals. The FFT processes for each ICA component data decomposed from 30 channels of the EEG signals and the processes are described as following. The sampling rate of EEG is 250Hz. The power spectrum density (PSD) of each ERP is evaluated with the spectral analysis process. The activity power spectrum of the ERP is calculated by averaging the PSDs. The ICA data power spectrum time series for each session consisted of ICA data power estimates at 50 frequencies (from 1 to 50 Hz).

The input EEG signal is $x[n]$. And we can consider computing $X[k]$ by separating $x[n]$ into two $(N/2)$ -point sequences consisting of the even-numbered points in $x[n]$ and the odd-numbered points in $x[n]$.

$$W_N^2 = e^{-2j(2\pi/N)} = e^{-j2\pi(N/2)} = W_{N/2} \quad (3)$$

The PSDs was calculated as following equations:

$$\begin{aligned} X[k] &= \sum_{r=0}^{(N/2)-1} x[2r]W_{N/2}^{rk} + W_N^k \sum_{r=0}^{(N/2)-1} x[2r+1]W_{N/2}^{rk} \\ &= G[k] + W_N^k H[k], \quad k = 0, 1, \dots, N-1, \end{aligned} \quad (4)$$

3.5 Event Related Spectral Perturbation Analysis

The Event Related Spectral Perturbation, or ERSP, was first proposed by Makeig [42]. ERSP, we are able to observe time-locked but not necessary phase-lock activities. It is different from the limitation of ERP. ERP must be coherent time-and-phase-locked activities. The ERSP measures average dynamic changes in amplitudes of the broad band EEG spectrum as a function of time following cognitive events.

The processing flow is shown in Fig. 3-6. The time sequence of EEG channel data or ICA activations are subject to Fast Fourier Transform (FFT) with overlapped moving windows. Spectrums in each epoch were smoothed by 3-windows (768 points) moving-average to reduce random error. Spectrums prior to event onsets are considered as baseline spectra for every trial. The mean baseline spectra were converted into dB power and subtracted from spectral power after stimulus onsets so that we can visualize spectral ‘perturbation’ from the baseline. This procedure is applied to all the epochs, the results are then averaged to yield ERSP image. The ERSP image mainly shows spectral differences after event, since the baseline spectra prior to event onsets have been removed.

After performing bootstrap analysis (usually 0.01 or 0.03 or 0.05, here we use 0.05) on ERSP, only statistically significant ($p < 0.05$) spectral changes will be shown in the ERSP images. Non-significant time/frequency points are masked (replaced with zero). Any perturbations in frequency domain become relatively prominent.

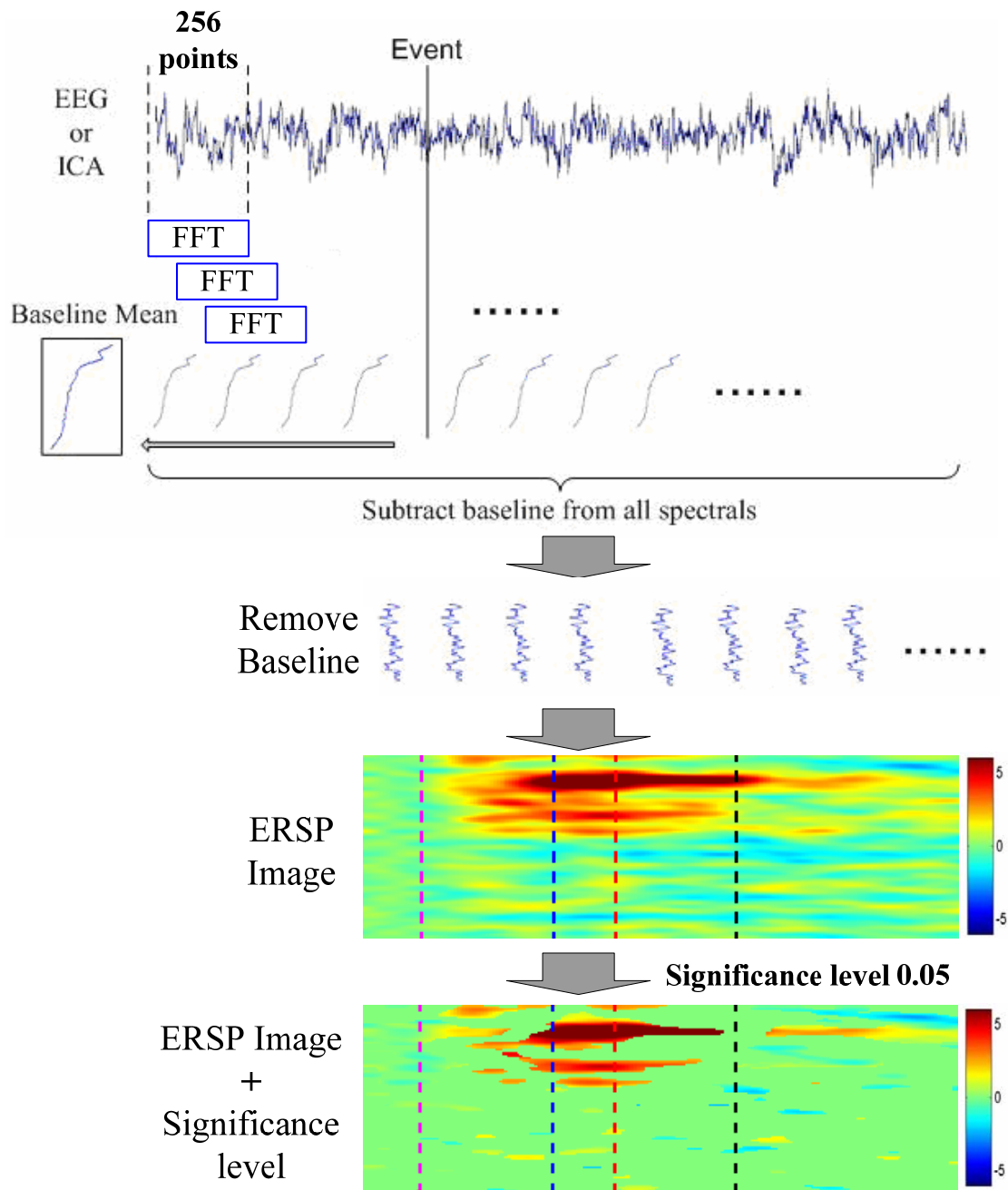


Fig. 3-6: The illustration of procedures in ERSP analysis. FFT was applied in each window with 256 samples, and there was 244-sample overlap of two adjacent windows. The time-dependent ERSP image was composed of the spectra of each window, and smoothed by 3-window moving average. In the final step, the significant parts of ERSP image were extracted by using bootstrap method. The pink dashed lines: the first event onset. The blue dashed lines: the averaged reaction time to the deviation. The red dashed lines: the averaged response time to math. The black dashed lines: averaged response time for the car returning to the third lane. Color bars showed the magnitude of ERSPs.

3.6 Component Clustering

To study the cross-subject component stability of ICA decomposition, components from multiple subjects were clustered based on their spatial distributions and EEG characteristics. But, components from different subjects thus may differ in many ways such as scalp maps, power spectra, ERPs and ERSPs. [43] [44] [45] attempted to solve this problem by calculating the similarities (distance) among different independent components. Components from multiple subjects were clustered in terms of their scalp maps and activation power spectra. Individual component clusters were characterized by their mean cluster map and activity spectrum. This method was also known as component clustering.

In this study, we attempt to completely components cluster. We used the K-means algorithm (EEGLAB 4.3) to analyze (as shown in Fig. 3-7). To cluster these components into small number (for instance, 10) of groups, one approach is to apply K-means on their scalp map and power spectral. In practice, we could hardly achieve such clean clusters if we relied entirely on K-means to classify components, since less than half of components were meaningful after ICA decomposition, others were usually account for noises. These components might confuse K-means algorithm and reduce the consistency of each clusters. Another problem arose from combining scalp map and power spectral information for K-means classification. It remained an open question how to weight the spatial information (scalp maps) and source activity, accounted for by power spectra in the K-means clustering. Therefore, we selected stable components which were classified iteration by K-means algorithm into 16 clusters in terms of component scalp maps (EEG.icawinv). Then we grouped 16 clusters into 7 significant clusters and discarded some non-significant clusters

manually based on power spectra of the components. The resultant clusters are named according to the source locations of components (as shown in Fig. 3-8).

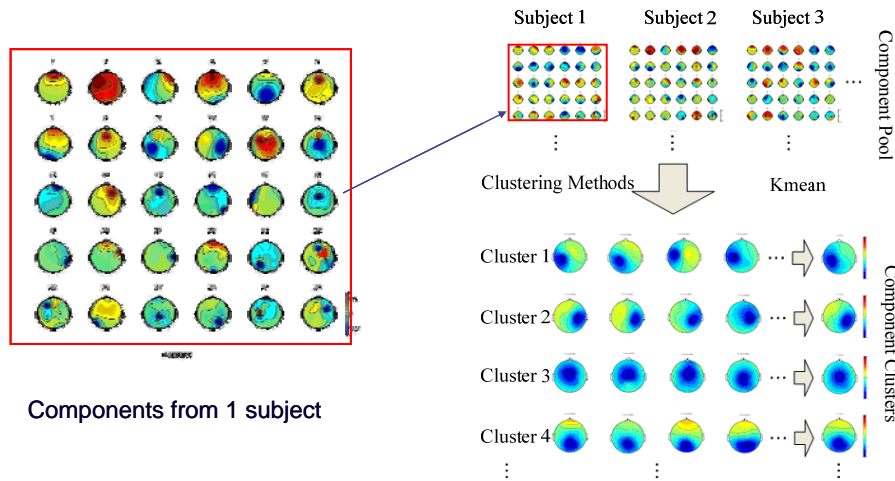


Fig. 3-7: The flowchart of component clustering by using K-means algorithm. Components from 11 subjects were classified into several significant clusters according to their K-means.

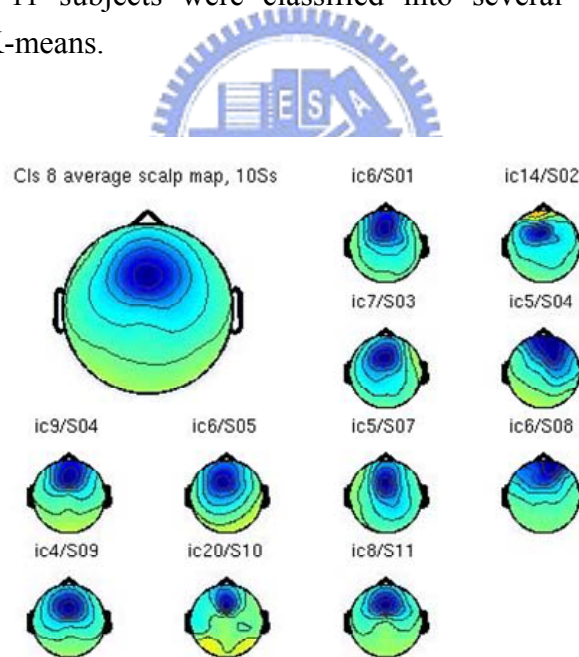


Fig. 3-8: The typical example of the component clustering result. The mean of scalp map was averaged across 11 subjects.

IV. Results

The EEG signals collected from 11 subjects were analyzed for the study of distraction. Each experiment included 4 sessions and each session lasted 15 minutes. Every session presented five cases randomly (designed with different time intervals between tasks). The influence of stimulus onset asynchrony in the subjects' behavior performance was studied in the first section. Then we characterized changes of dynamic brain activities from the independent component clusters and the power spectrum and the event-related spectral perturbations (ERSPs) under different cases. The following paragraphs showed detailed results.

4.1 Behavior Performance



The response time of the tasks (the deviation and the math) was collected to study behavior of the subjects in the experiments. The outliers were first removed from the 11 subjects' behavior data. By using one way ANOVA, the significance of the behavior data were tested for every subject. The testing results were showed in Fig. 4-1. The response time to deviation was given in Fig. 4-1(A). The blue bars were in the figures represented the case of math-400ms-deviation (case-1), the light blue bars were represented the case of math-deviation (case-2), the yellow bars were represented the case of deviation-400ms-math (case-3), and the red bars were represented the case of single-deviation (case-5).

The response time to deviation in case-5 (single deviation) was significantly larger than that in the case-1 (math present 400 ms before deviation) for most of the subjects (8 out of 11). The response time to deviation in case-5 (single deviation) was

significantly larger than that in the case-2 (two tasks present at the same time) for four subjects. And, the response time to deviation in case-5 (single deviation) was significantly larger than that in the case-3 (deviation present 400 ms before math) for only one subject. These results were shown in Fig. 4-1(A). This meant it take longer time for the subjects to reply to the driving task in single deviation case. Because when the deviation task appeared in the case-1 subjects were in order to continuously resolve the mathematical equations, they had to firstly and rapidly response to the deviation task to avoid hitting the wall.

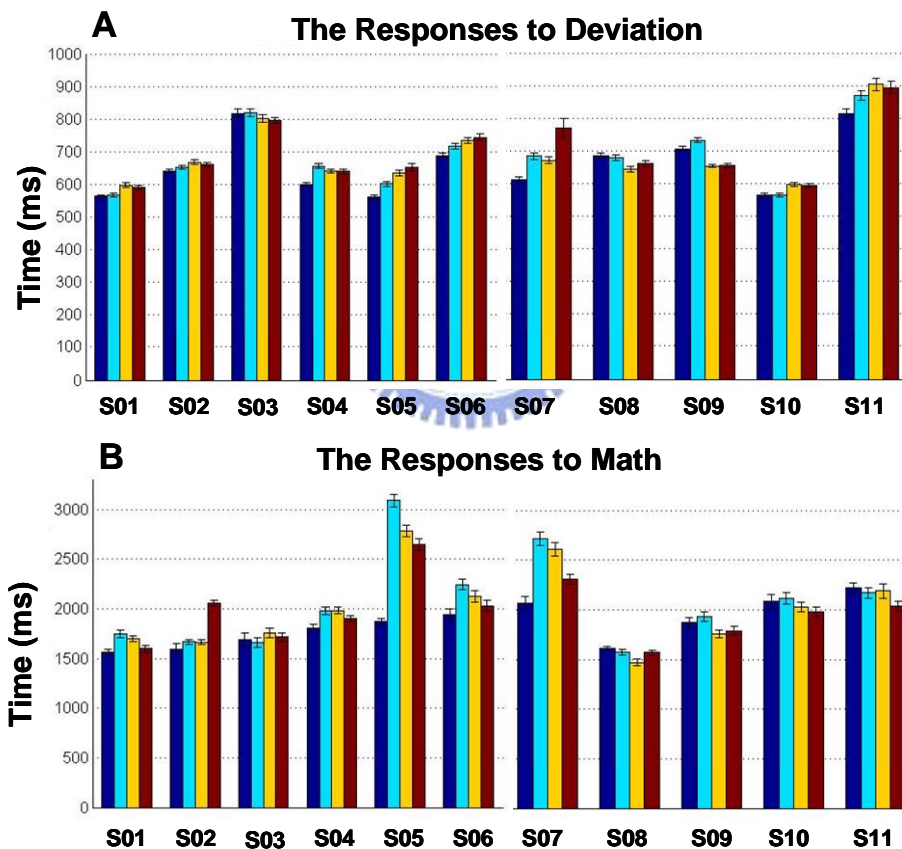


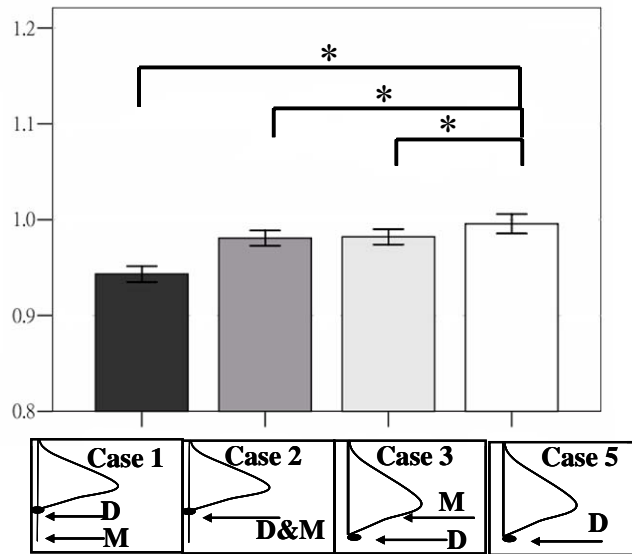
Fig. 4-1: Bar charts of the averaged response time to the deviation (A) or the math (B) onsets between four cases. The blue bars: case-1 (the math occurred at 400ms before the deviation onset); the light blue bars: case-2 (the math and deviation occurred at the same time); the yellow bars: case-3 (the math occurred at the 400 ms after the deviation onset); and the red bars: case-4 (only presented the math question in this case) or case-5 (only deviation occurred in this case).

In Fig.4-1 (B), the response time to math in case-4 (single math) was significantly shorter than that in the case-1 (math present 400 ms before deviation) for most of the subjects (7 out of 11). The response time to math in case-4 (single math) was significantly shorter than that in the case-2 (two tasks present at the same time) for six subjects. And, the response time to math in case-4 (single math) was significantly shorter than that in the case-3 (deviation present 400 ms before math) for four subjects. This meant it take shorter time for the subjects to reply to the math task in single math case.

In order to investigate the overall of behavior index, we used the technology of nonparametric tests. The nonparametric analysis was used because several extremely large scores significantly skewed. First, the data was randomly selected the trials which there was the same trials in all cases. Then, the response time of the two tasks in the five cases were normalized to the single-deviation and single-math tasks. We used the Statistical Package for Social Science (SPSS) for Friedman test, and the result was shown in Fig. 4-2.

The normalized response time to deviation was given in Fig. 4-2(A). The response time to deviation for dual tasks (case-1 to case-3) were significantly shorter than that for the single task (case-5). There were no statistical significant differences between the case-2 and the case-3. The largest response time to the deviation onset was the case-5. The normalized response time to math was given in Fig. 4-2(B). The response time to math presented for dual tasks (case-1 to case-3) were significantly longer than that for the single task (case-4). There were no statistical significant differences between case-1 and case-2. The shortest response time to the math onset was the case-4.

A The Responses to Deviation



B The Responses to Math

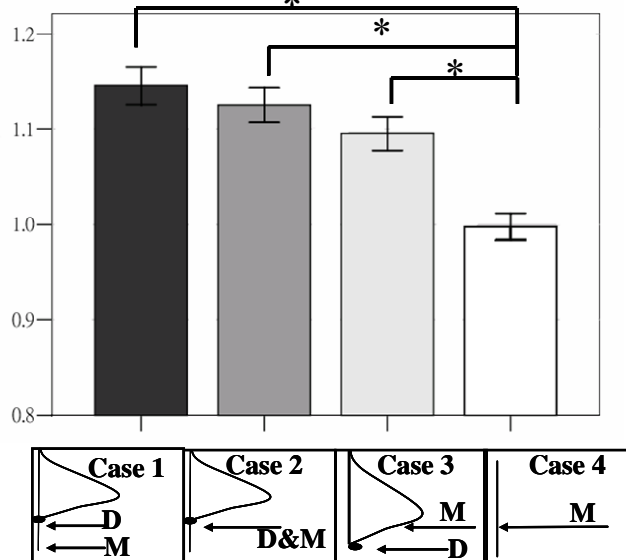


Fig. 4-2: Bar charts of normalized response time to the deviation (A) and math (B) presented between 5 cases across 11 subjects. The filled black bar: case-1; dark gray bar: case-2; light gray bar: case-3; the opened bar: single case. The bottom insets showed the onset sequences between two tasks. Note: the response time to deviation for dual tasks (case-1 to case-3) were significantly shorter than that for the single task (case-5). The largest response time to the deviation onset was the case-5. The response time to math presented for dual tasks (case-1 to case-3) were significantly longer than that for the single task (case-4). The shortest response time to the math onset was the case-4.

Further, we wanted to know the difference which cases was made. Then, Post Hoc test was to use Student-Newman-Keuls test, and the result was shown in Table-3.

The explanations were showed below.

(1) Normalized response time to deviation:

The result of test statistic was $\chi^2_{0.05,3} = 16.04$ from Friedman test, and $p=0.000 < 0.05$. Therefore, the result rejected the null hypothesis. In the analysis, we found the four cases (case-1, case-2, case-3, and case-5) significantly different with each other. Using Student-Newman-Keuls test, we found three significant groups (case-1, case-2 and case-3, case-5).

(2) Normalized response time to math:

The test statistic was $\chi^2_{0.05,3} = 148.859$ from Friedman test, and $p= 0.000 < 0.05$. The four cases (case-1, case-2, case-3, and case-5) were significantly different with each other. And, we used Student-Newman-Keuls test to also find three significant groups (case-1 and case-2, case-3, case-4).

Table-3 the normalized response time to deviation and math

Case	Response time to deviation			Response time to math		
	Mean	(SD)	Difference (dual-single)	Mean	(SD)	Difference (dual-single)
Case 1	1.216864	0.151223	-0.07 p<0.01	1.891619	0.509387	0.23 p<0.01
Case 2	1.265610	0.157821	-0.02 p<0.01	1.860181	0.472608	0.2 p<0.01
Case 3	1.269600	0.169142	-0.01 p<0.01	1.811820	0.478367	0.15 p<0.01
single(baseline)	1.287392	0.211970		1.659849	0.413884	

4.2 EEG Results of the Dual-Task Experiment

4.2.1 Distraction-Related Brain Sources

EEG epochs were extracted from the recorded EEG signals after down sampling, filter and artifact removal. We used ICA to decompose the independent brain sources from EEG signals. Fig. 4-3 showed the scalp topographies of ICA back-projection matrix W^T . As shown in Fig. 4-3, most of the EEG artifacts and channel noises in EEG recordings were effectively separated into ICA components 1, 2, 29 and 30, while ICA components 3, 4, 9, 10, 11 and 12 (selected by visual inspection) may be considered as effective “sources” associated with distraction in the dual-task driving experiment. Fig. 4-3 showed the components we were interested in, which were selected based on their characteristic scalp maps, dipole source locations, spectral signatures, and within subject consistency.

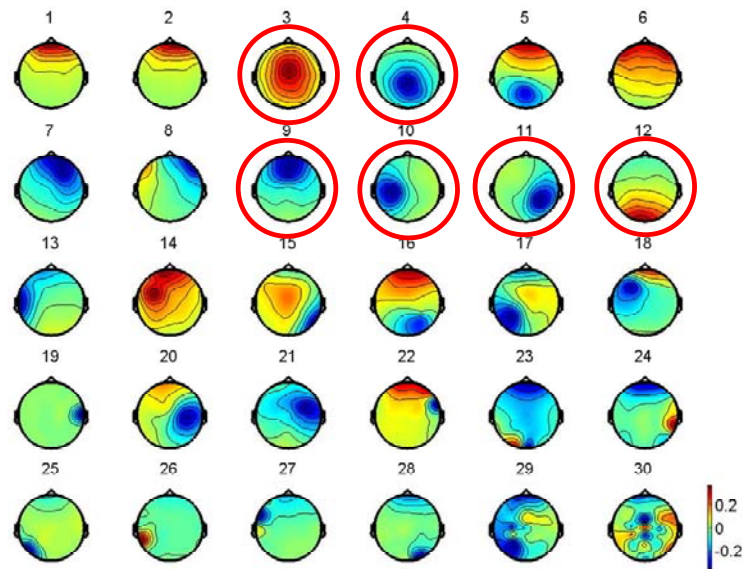


Fig. 4-3: Scalp map topographies of ICA decomposition of subject-4. The selected components (by visual inspection) were central midline (3), parietal (4), frontal (9), motor (10 and 11) and occipital (12) components. The color bar showed the amplitude of component signals.

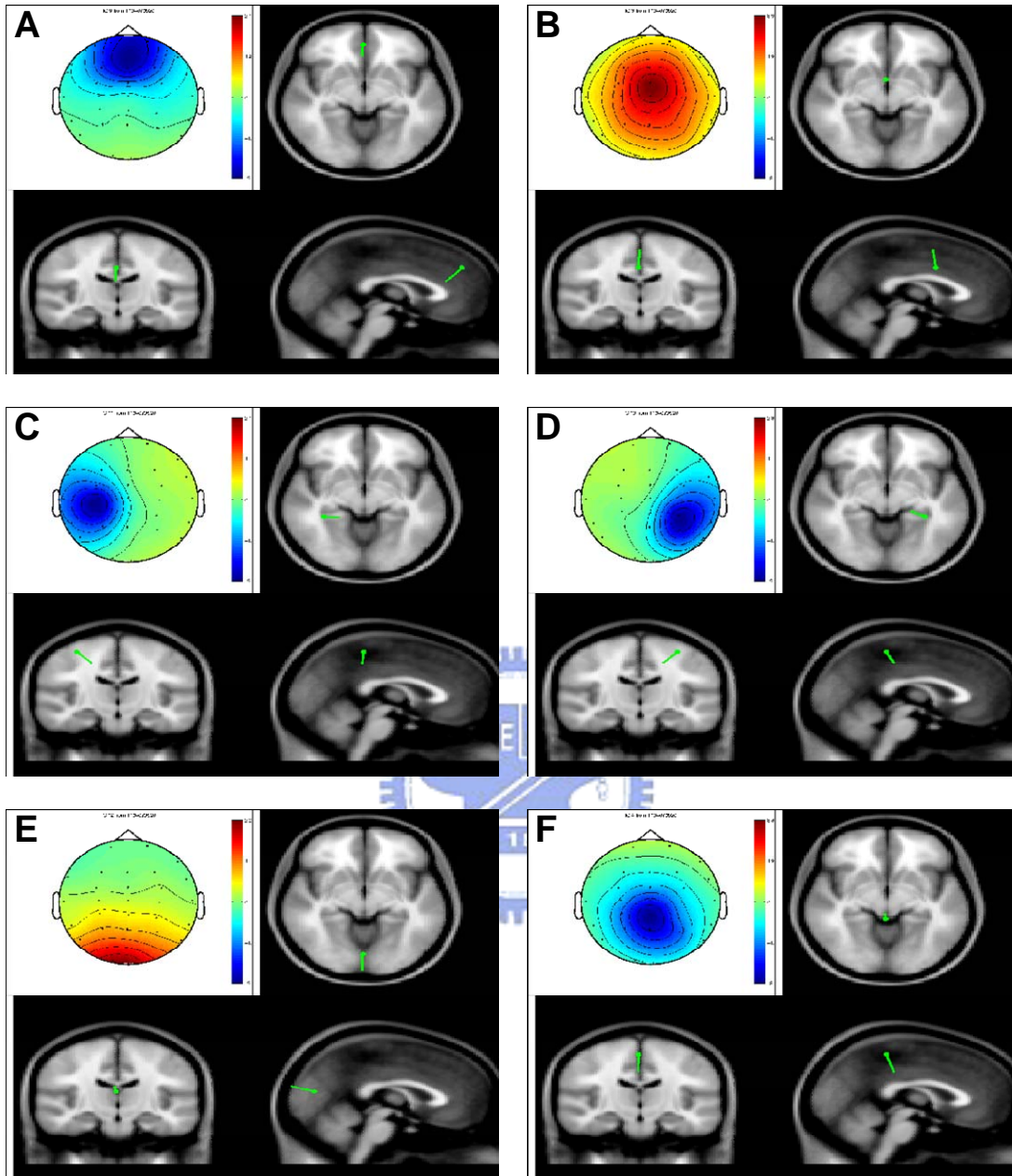
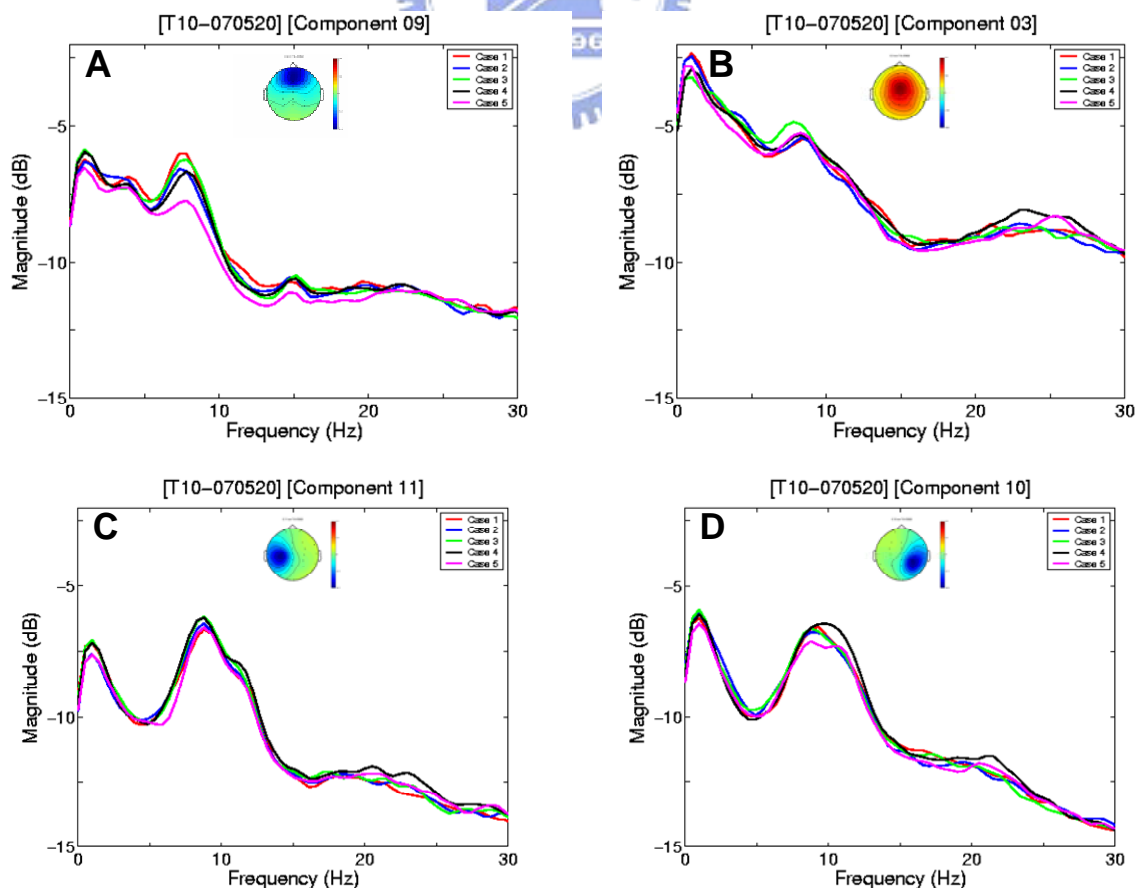


Fig. 4-4: The illustration of the component maps and their corresponded dipole locations of the frontal (A), the central midline (B), the left motor (C), the right motor (D), the occipital (E) and the parietal (F) area. The left upper panels: the scalp maps. The right upper panels: the top viewing angle of dipole source location. The left lower panels: the coronal viewing angle of dipole source location. The right lower panels: the sagittal viewing angle of dipole source location. Color bars: the amplitude of component signals.

Plenty of brain sources were involved in the distraction driving experiments. For example, the motor area (components 10 and 11) would be activating when the subject was trying to control the car with the steering wheel, and activations in the frontal area (component 9) were related to attention. Therefore, ICA components including central, frontal, parietal, motor and occipital lobe were selected for further analysis. The component map topography and the dipoles related to the selected components were shown in Fig. 4-4.

The power spectra related to different cases were compared as shown in Fig. 4-5 to determine the distraction-related components. The difference in power spectra between cases could be observed in several components, such as the significant power increases near the theta band (5 ~ 7.8 Hz) of the frontal component were showed in the dual tasks (as shown in Fig. 4-5 (A)).



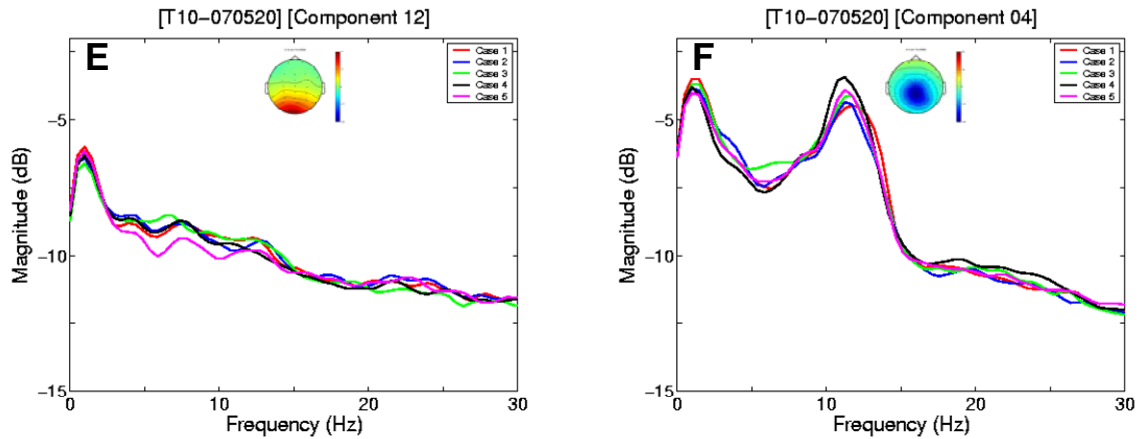


Fig. 4-5: Illustration of the typical example of six ICs and their power spectra from five different cases in the frontal component (A), central midline component (B), left motor component (C), right motor component (D), occipital component (E), and the parietal component (F). Red line: case-1, blue line: case-2, green line: case-3, black line: case-4, pink line: case-5. Note: comparing with the single task, the significant power increases near the theta band (5 ~ 7.8 Hz) of the frontal component were showed in the dual tasks.

We further compared the ICA power spectra between single- and dual-task cases, the results were shown in Fig. 4-6, 4-7, 4-8 and 4-9. The black curves in these figures represented the ICA power spectrum of single-task cases. The subplots (A), (B) and (C) displayed in the left column showed the comparison between the single math case and three dual-task cases and the subplots (D), (E) and (F) displayed in the right column showed the comparison between the single deviation case and three dual-task cases.

The ICA spectrum comparisons between single- and dual-task cases in the central midline component were given in Fig. 4-6. There were no apparently differences observed in the total power spectra among cases.

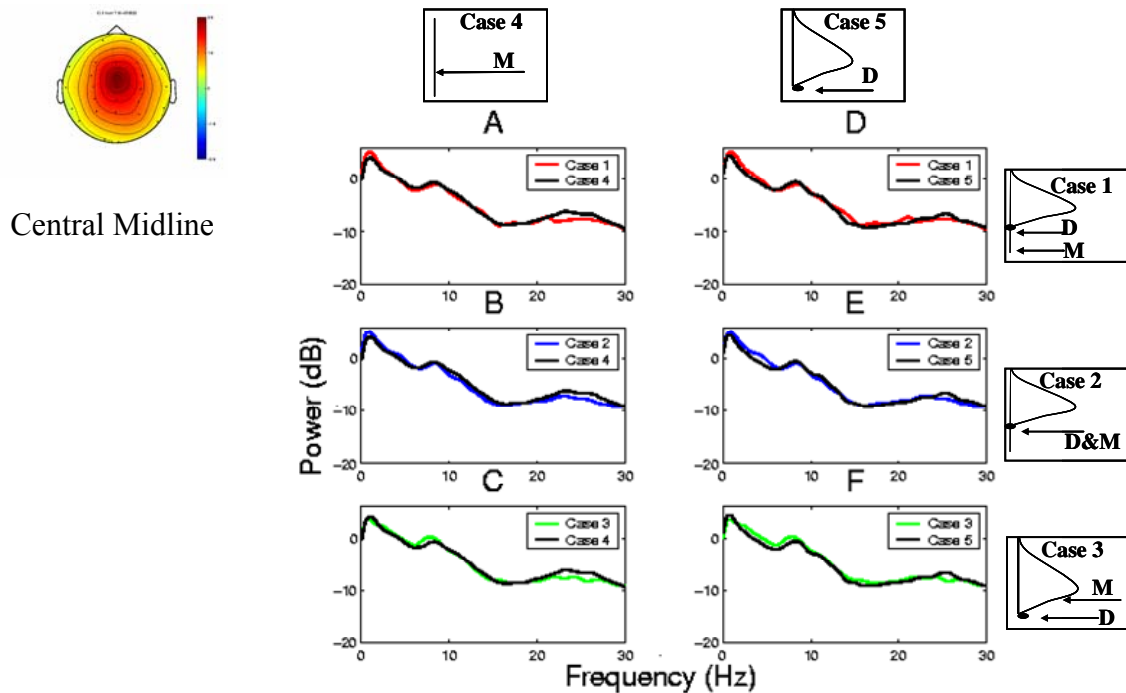


Fig. 4-6: Single subject data. The comparison of total power spectra between single- and dual-task in the central midline component. Left column (A-C) showed the comparison between the case of single math and three dual-task cases. Right column (D-F) showed the comparison between the case of single deviation and three dual-task cases. The right column and the upper row insets showed the onset sequences between two tasks. The left block: scalp map for the central midline component of subject-4. Red line: case-1, blue line: case-2, green line: case-3, black line: case-4 or case-5. Note: There were no apparently differences observed in the total power spectra among cases.

The ICA spectrum comparisons between single- and dual-task cases in the motor component were given in Fig. 4-7. In the figures, we found a peak in 10 Hz band for all cases. The peak was induced during increasing force output in motor activity. Different spectra were observed between the case of single math and three dual-task cases. In comparison with the single task, the powers of the alpha band were weaker in the dual tasks. These maybe induced by distracted.

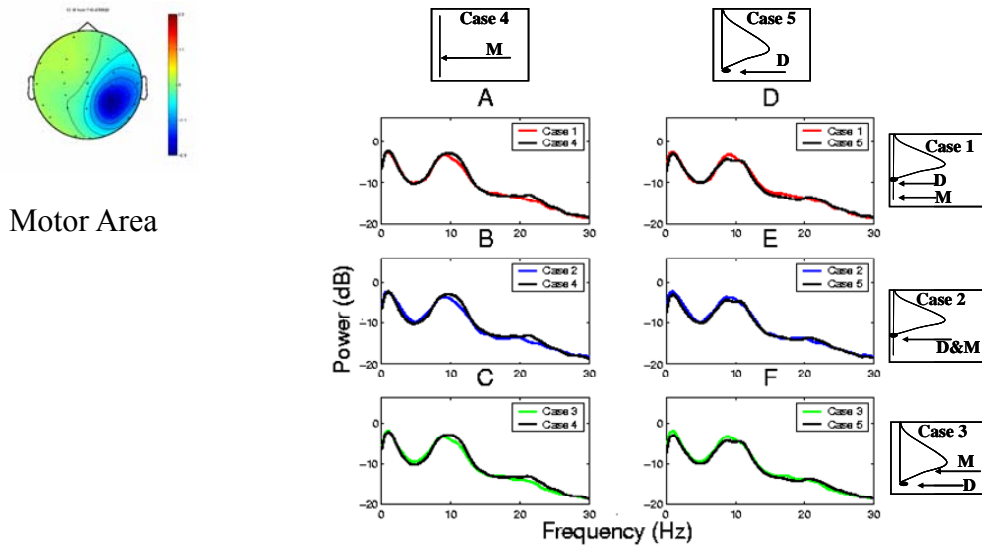


Fig. 4-7: Single subject data. The comparison of power spectral baselines between single- and dual-task cases in the motor component. Panels as Fig. 4-6. Note: a 10-Hz peak observed in all cases. Different spectra were observed in left column (A-C). In comparison with the single task, the powers of the alpha band were weaker in the dual tasks.

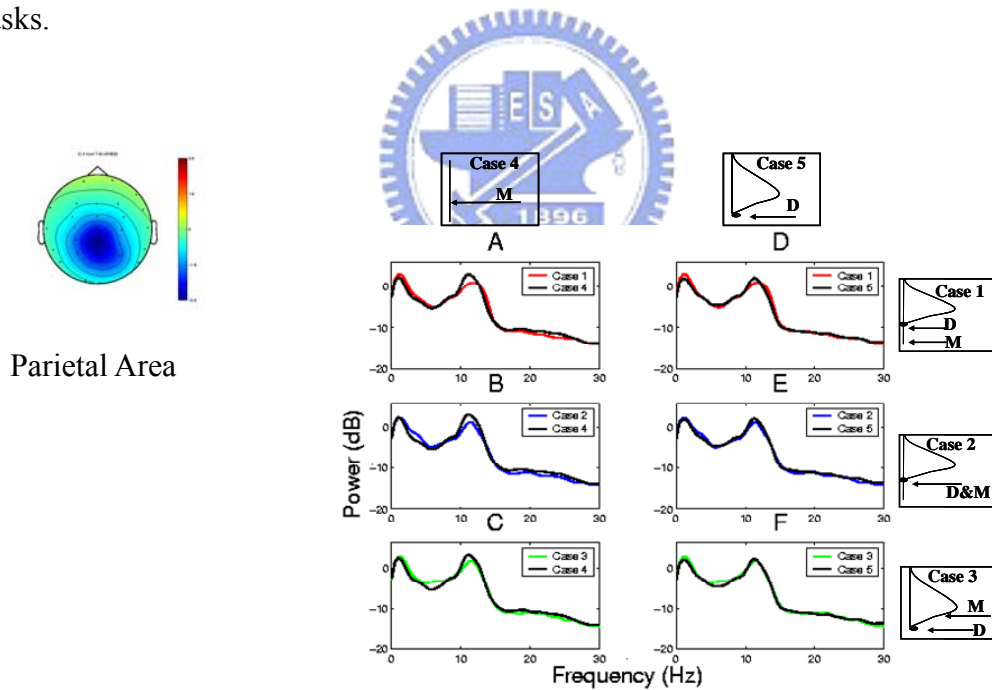


Fig. 4-8: Single subject data. The comparison of power spectra between single- and dual-task cases in the parietal component. Panels as Fig. 4-6. Note: a 10-Hz peak observed in all cases. Different spectra were observed in left column (A-C). In comparison with the single task, the powers of the alpha band were weaker in the dual tasks.

In Fig. 4-8, we found that a 10-Hz peak observed in all cases. Different spectra were observed between the case of single math and three dual-task cases. In comparison with the single task, the powers of the alpha band were weaker in the dual tasks. Because the parietal component was close to the motor area, thus we inferred that power change was the same in two components. Therefore, we could use another analysis (such as ERSP) to look at the difference in 10 Hz band.

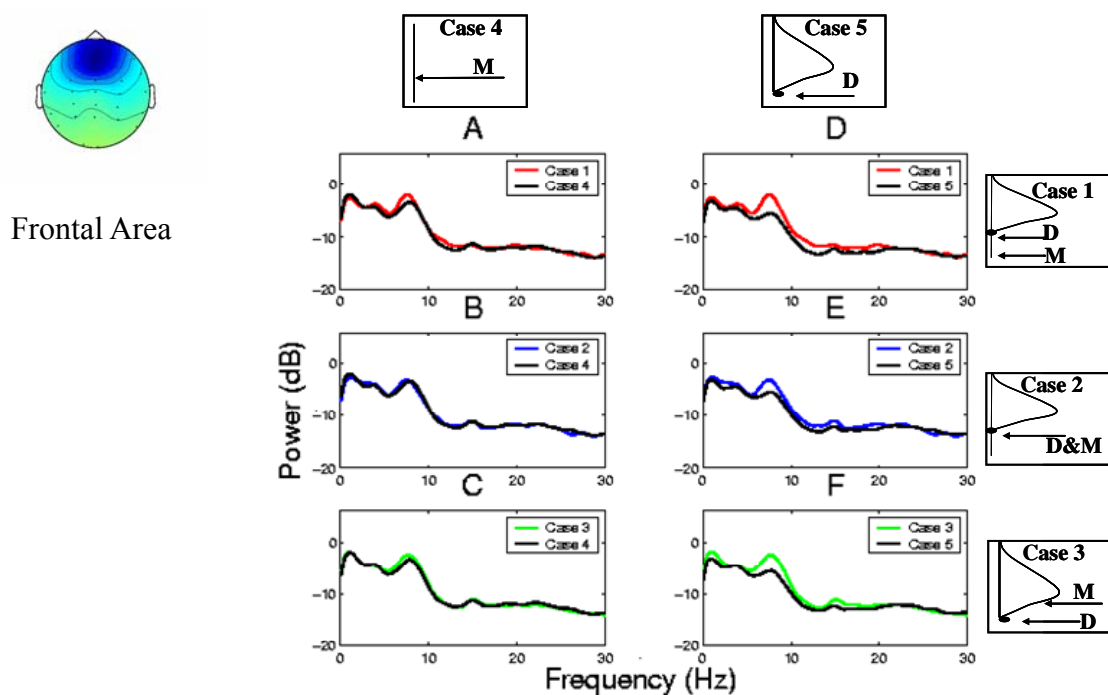


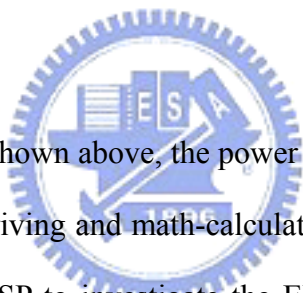
Fig. 4-9: Single subject data. The comparison of power spectra between single- and dual-task cases in the frontal component. Panels as Fig. 4-6. Note: comparing with the single deviation, the significant increases of power spectra were observed around 5 to 10 Hz in the dual-task cases (D-F).

The comparison of power spectra between single- and dual-task cases in the frontal component were given in Fig. 4-9. Comparing with the single deviation, the significant increases of power spectra were observed around 5 to 10 Hz in the dual-task cases. The activation in frontal areas was induced by mathematics and mental task which were reported in many previous studies. The phenomena in our

experiment were also to find. Significant power increases were observed between the single-deviation and the dual-task cases as shown in Fig. 4-9 (D), (E), (F).

According to the results shown in these figures, we found that the spectra in motor component were difference between the single-math and the dual-task cases in 10 Hz band. Then it was considered as the dominant component to the deviation task. The spectra in frontal component were difference between the single-deviation and the dual-task cases in 5~10 Hz band and the frontal component were considered as the dominant component to the math task.

4.2.2 Event Related Spectral Perturbation Results in Single Subject



According to the results shown above, the power differences in motor and frontal components were related to driving and math-calculation tasks, respectively. We then applied the technology of ERSP to investigate the EEG responses in both time and frequency domains. Event Related Spectral Perturbation (ERSP) plotted the grand mean time course of changes from pre-stimulus baseline in log spectral power of a scalp-recorded EEG or ICA component activation time-locked to stimulus presentation or subject responses across frequencies. Through ERSP, we were able to observe time-locked but not necessarily phase-locked activities.

4.2.2.1 ERSP Results in Frontal Component

The ERSP plot of the single math cases of the frontal component was shown in Fig. 4-10(a). The pink dashed lines in the figures were representing the event onset and the red dashed lines indicated when was the subject response to the event with

pressing a button (i.e. the mathematic equations). The significance of the top plot of ERSP in the figure were tested ($p < 0.05$) and shown in the bottom figure.

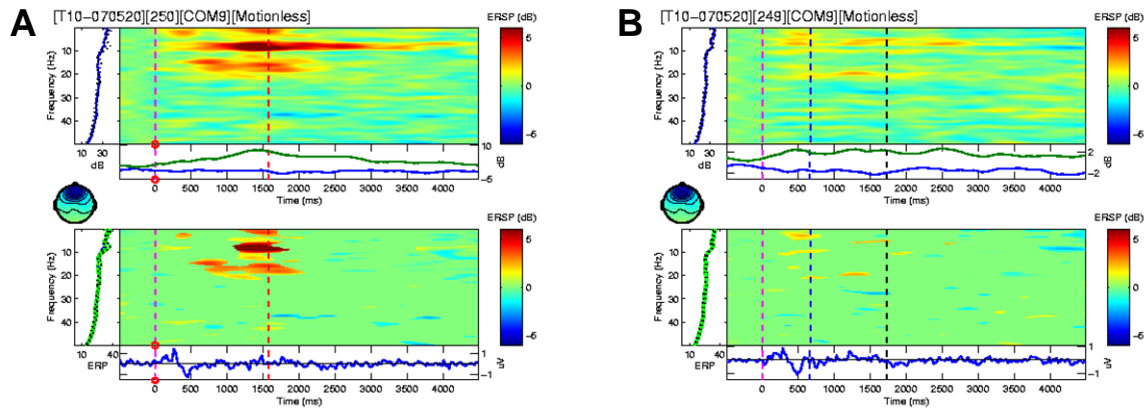


Fig. 4-10: Single subject data. The ERSP plots of the single-task cases in the frontal component. The significance of the top plot of ERSP in this figure were tested ($p < 0.05$) and shown in the bottom figure. (A) single-math task. (B) single-deviation task. The pink dashed lines were showed the onset of the first event; the red dashed lines indicated averaged response time to the math; the blue dashed lines indicated averaged response time to the deviation and the black dash lines indicated the averaged response time for subjects steering the car back to the third lane.

A significant power increase time-lock to the mathematic equation onset was observed in the frontal component shown in Fig. 4-10 (A). The ERSP plot of the single deviation case of the frontal component was shown in Fig. 4-10 (B). There was no significant power increase observed in the frontal component in the single deviation case. These results again demonstrated that the frontal component was the dominant component of the mathematic calculation in human brain.

We then focused on the ERSP responses in the frontal component when the mathematic and the deviation task were presented to the subject (i.e. the dual-task cases). The ERSP plots of the dual-task cases were given in Fig. 4-11. Significant power increases were observed in the three cases in the frontal component since the

mathematic task was presented to the subjects in these three cases. The ERSP shown in Fig. 4-11 (A) was the EEG power response when the math was presented at 400ms before deviation; Fig. 4-11 (B) showed the ERSP results when the two tasks were presented at the same time and Fig. 4-11 (C) showed the ERSP results when the math was presented at 400ms after deviation. The red dot represents the onset of math event and blue circular represented the onset of deviation event. From the ERSP images we found the significant power increase time-locked to mathematic equation onsets (red dot).

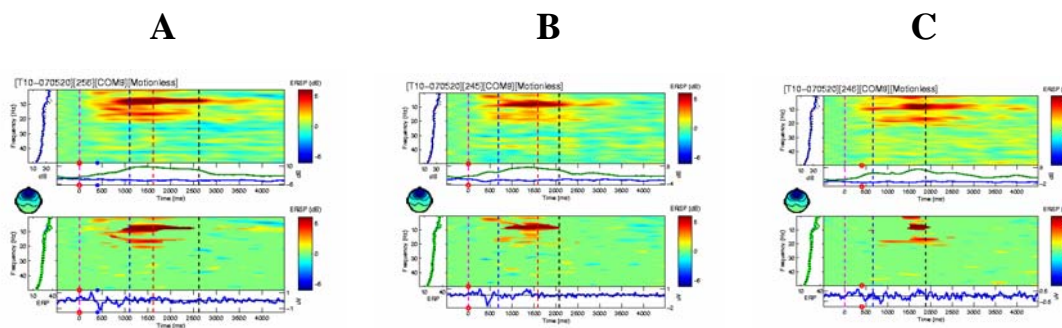


Fig. 4-11: Single subject data. The ERSP plots of the dual-task cases in the frontal component. Panels as Fig. 4-10. Comparing with the single task, significant power increases around theta band (5~7.8 Hz) and beta band (12.2~17 Hz) were observed in the three cases. Case-1 (A), case-2 (B) and case-3 (C).

In order to investigate the distracted effect of stimulus onset asynchrony, five cases were designed in this experiment. The ERSP images corresponding to the five cases in the frontal component were compared in Fig. 4-12. We had demonstrated that the power increase in the frontal component was related to math-task. Thus in case-1~4, significant power increases in theta band were observed. The power increases in the three dual-cases including case-1, case-2 and case-3 were slightly different to each other. The difference might caused by the time of SOA. In Fig. 4-12, the power increase in case-1 was significantly larger than in case-2 and case-3.

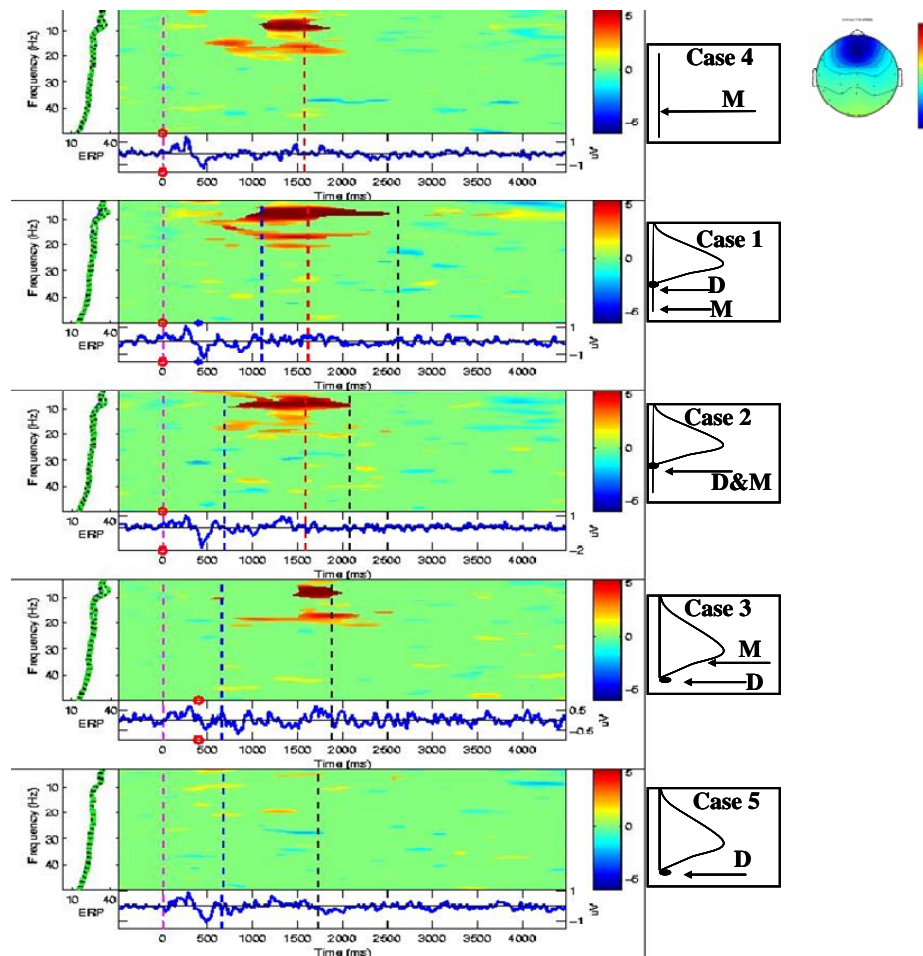


Fig. 4-12: Single subject data. The ERSP plots of the five cases in the frontal component. The right column: the scalp map of the frontal component for five cases. The middle columns showed the onset sequences between two tasks. Color bars showed the power of ERSPs. Pink dashed lines: the event onset. Blue dashed lines: the mean of reaction time to deviation. Red dashed lines: the mean of reaction time to math. Black dashed lines: the averaged response time for subjects steering the car back to the third lane. Red dot: the onset of math events. Blue dot: the onset of deviation events. Note: the power increase in case-1 was significantly larger than in case-2 and case-3.

4.2.2.2 ERSP Results in Motor Component

As we mentioned before, the motor component was considered as the dominant component to the deviation task according to the results of power spectrum comparison. The ERSP plots of the single-math and single-deviation cases of the left

motor component were shown in Fig. 4-13 (A) and (B). Since the left and right motor components were the same phenomena, then here we selected the left motor component to present. The pink dashed lines in Fig. 4-13 were representing the event onset, the blue dashed lines indicated when was the subject response to the event (i.e. the deviation), and the black dashed line indicated when was the car back in the third lane with the control of the subject.

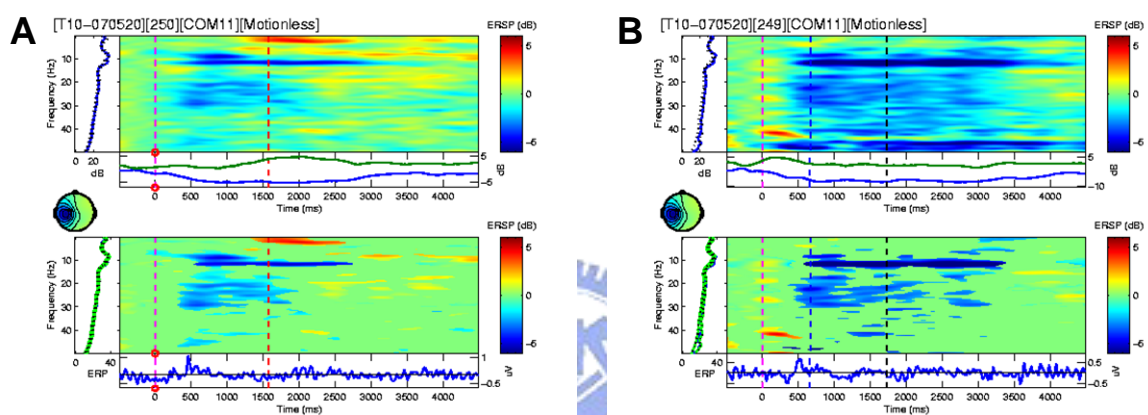


Fig. 4-13: Single subject data. The ERSP plots of the single-task cases in the motor component. Panels as Fig. 4-12. Note: the motor component was the dominant source of the motor control in human brain.

The ERSP plot of the single-math case of the frontal component was shown in Fig. 4-10(a). There was power change observed in the motor component in the single math case and the mu blocking appeared before the red line. This was induced by pressing a button. Similarly, but the phenomena was weak. Contrarily, a significant power suppression time-lock to the deviation onset was observed in the motor component as shown in Fig. 4-13 (B). These results demonstrated that the motor component was the dominant source of the motor control in human brain. We then focused on the ERSP responses in the motor component when both the mathematic and the deviation tasks were presented to the subject (i.e. the dual-task cases). The

ERSP plots of the dual-task cases were given in Fig. 4-14.

The ERSP images corresponding to the five cases in the motor component were compared in Fig. 4-14. We found alpha suppression in all cases time-locked to the event onsets. Because it could be suppressed by a simple motor activity such as clenching the fist of the contra lateral side, or passively moved. Similarly, we found maximal alpha suppression in the case of single deviation. Due to subjects just to do one task which steer wheel. But the duration of alpha suppression in three dual-task cases was longer than the duration of alpha suppression in the case of single. This might be because the subjects were influenced by the second task when they are trying to complete the first task.

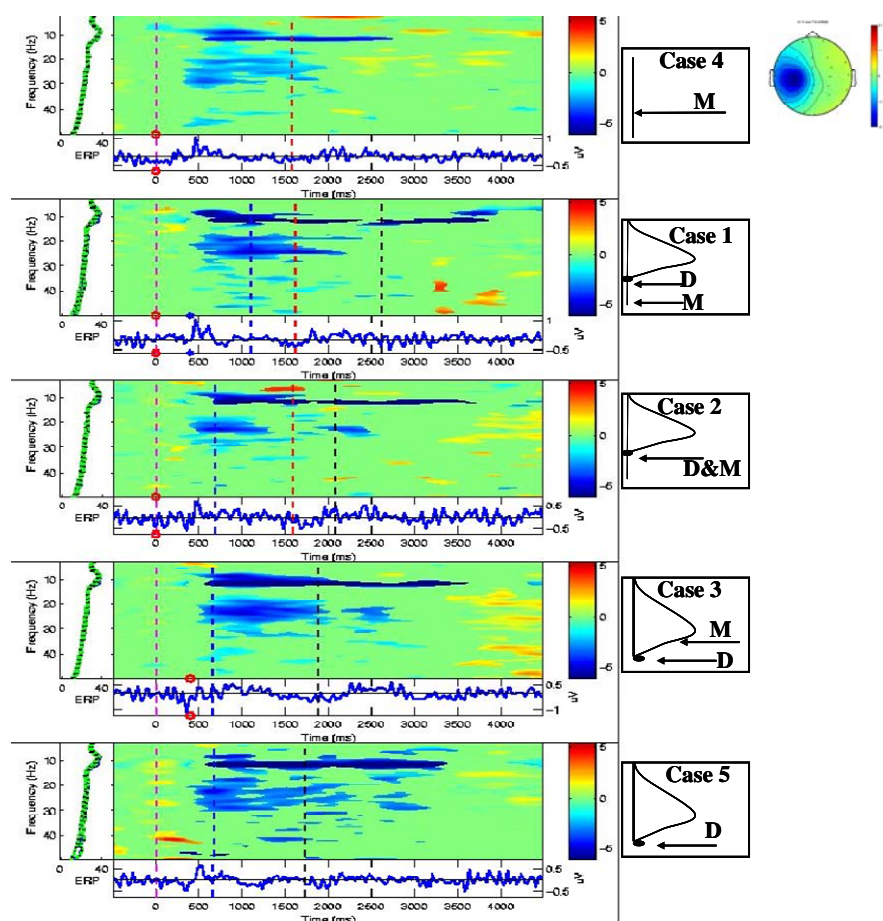


Fig. 4-14: Single subject data. The ERSP plots of the five cases in the motor component ($p < 0.05$). Panels as Fig. 4-12. Note: the alpha suppression briefly showed after the onsets of event were revealed in all cases. The maximal alpha suppression was observed in the case-5.

4.2.2.3 ERSP Results in Parietal Component

Since the parietal component was closer to the motor area, thus power suppression in alpha band was observed (as shown in Fig. 4-15). In Fig. 4-15, we found alpha suppression in all cases and the latency of the appeared alpha suppression are almost the same in all cases, and then we could explain that is time-locked to event-onset. The ending of alpha suppression was almost in black lines which was the car back in the third lane with the control of the subjects.

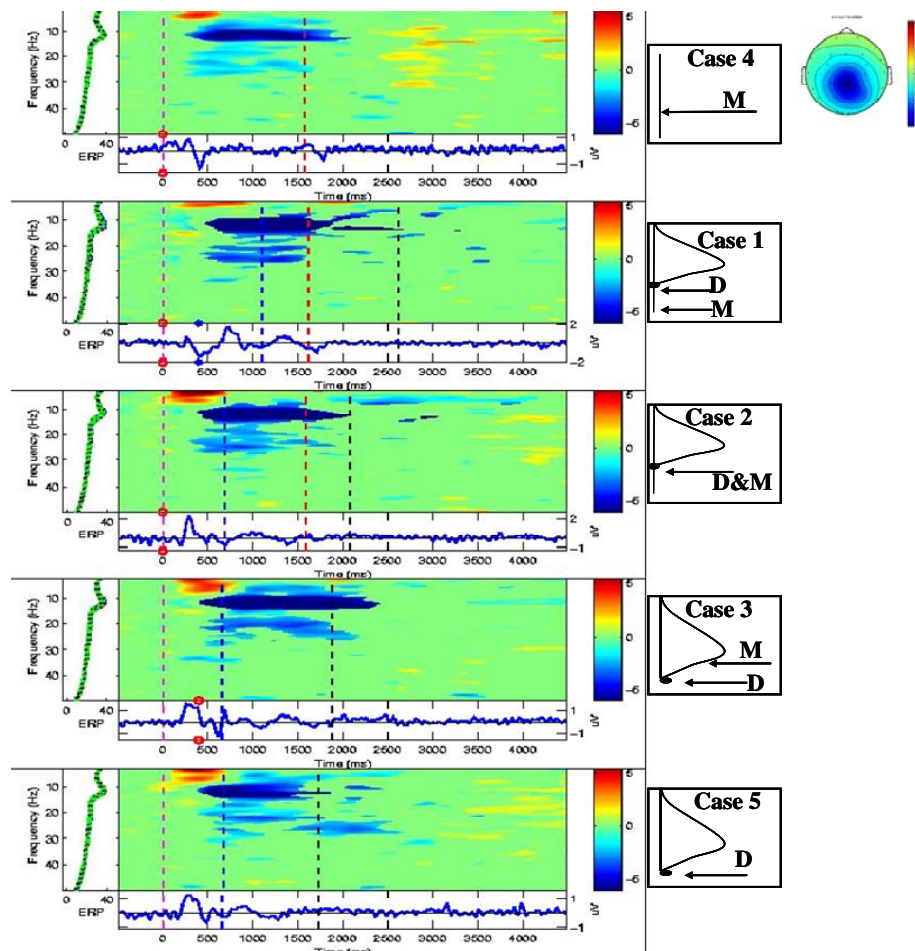


Fig. 4-15: Single subject data. The ERSP plots of the five cases in the parietal component ($p < 0.05$). Panels as Fig. 4-12. Note: the alpha suppressions time-locked to event onsets were observed in all cases.

4.2.2.4 ERSP Results in Occipital Component

Fig. 4-16 was showed occipital component. In Fig. 4-16, we found the ERPs were induced by the onset of math presented. The phasic power increases briefly after the onset of the math occurred around lower frequency band (0~8 Hz) was displayed in cases-1 to -4. The pattern maybe induced by visual stimulus. The red dashed lines indicated when was the subject response to the event with pressing a button (i.e. the mathematic equations). We also found alpha increase after red dashed lines in the cases with mathematical events; this was called rebound which subjects press a button to relax.

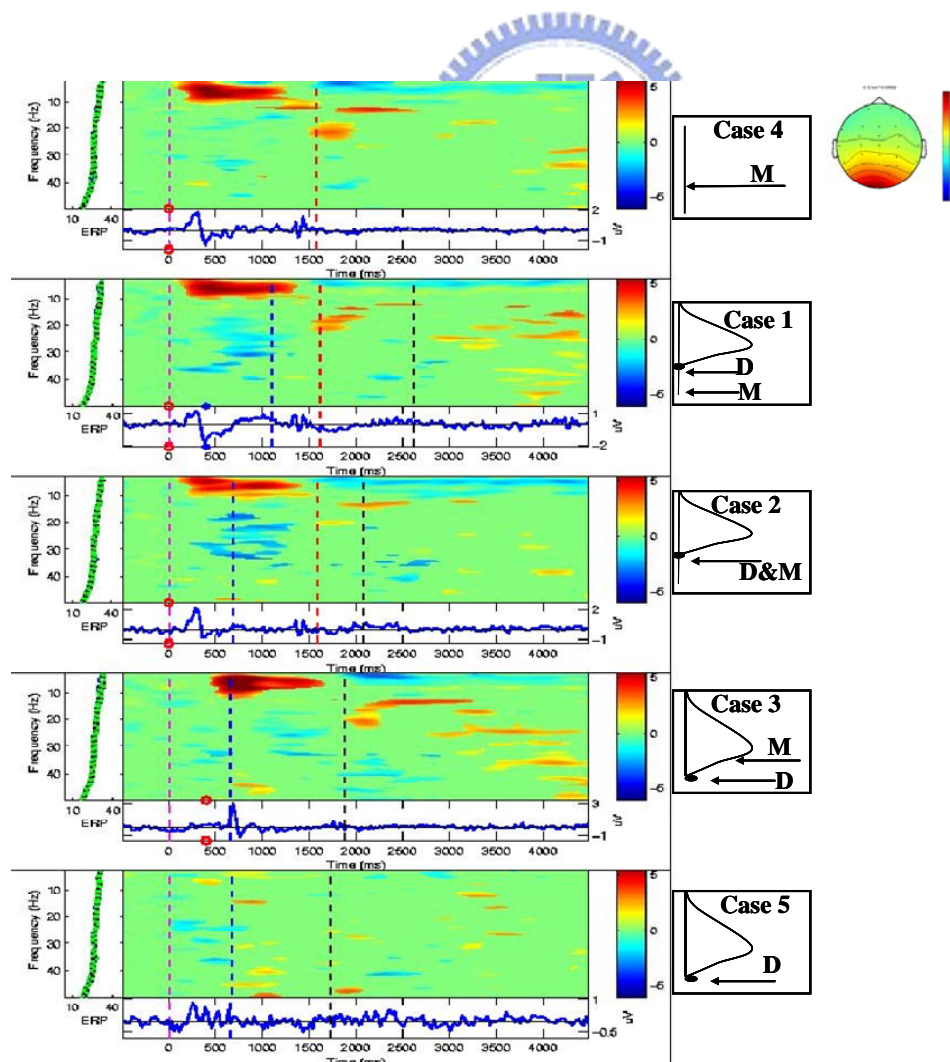
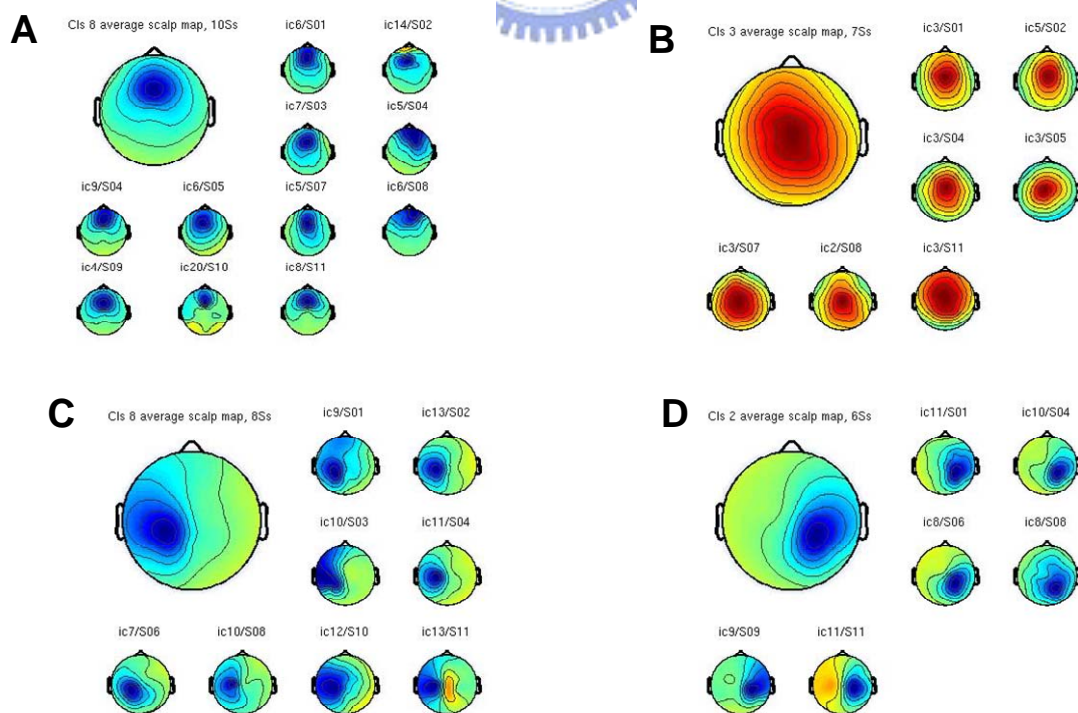


Fig. 4-16: Single subject data. The ERS/ERSP plots of the five cases in the occipital component ($p < 0.05$). Panels as Fig. 4-12. Note: the ERPs were induced by the onset of math presented. The phasic power increases briefly after the onset of the math occurred around lower frequency band (0~8 Hz) was displayed in cases-1 to -4.

4.2.3 Independent Component (IC) Clustering

To study the cross-subject component stability of ICA decomposition, components from multiple sessions and subjects were clustered based on their spatial distributions and EEG characteristics. Component clustering grouped massive components from multiple sessions and subjects into several significant clusters. Cluster analysis, k-means, applied to the normalized scalp topographies and power spectra of all 330 (30 channels x 11 subjects) components from the 11 subjects (see Data Analysis), and identified at least 7 clusters of components having similar power spectra and scalp projections.



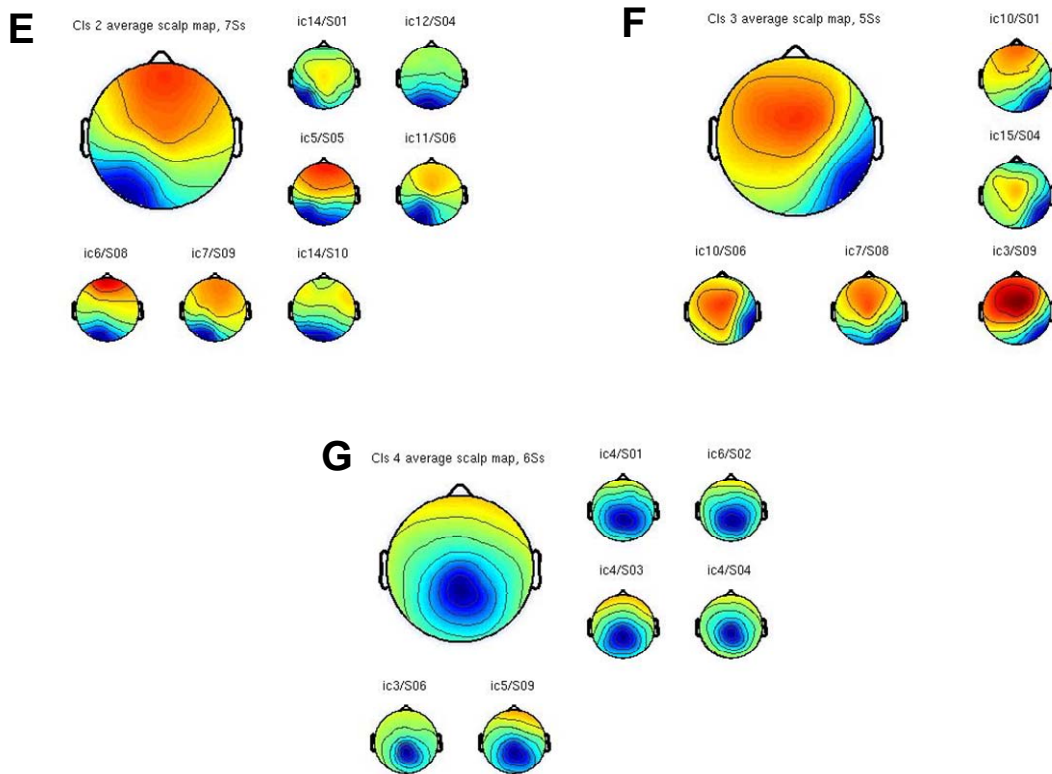


Fig. 4-17: The scalp maps for the frontal (A), central midline (B), left motor (C), right motor (D), parietal (E), left occipital (F) and the right occipital (G) independent component (IC) clusters across 11 subjects. Upper panels: the grand mean of the component map. Lower panels: individual scalp maps for the corresponded IC cluster.

These component clusters also showed functionally distinct activity patterns. Seven distinct component clusters (as shown in Fig. 4-17) accounted for frontal, central midline, parietal, left/right motor and left/right occipital, respectively. These were effectively removed from the activity of the other component clusters by the ICA decomposition and are not further considered here.

The numbers of components in different clusters were given in Table-5. The following group EEG responses were studied base on the results of component clustering.

Table-4: The Number of Components in Different Clusters

	Frontal	Central Midline	Parietal	Left Motor	Right Motor	Left Occipital	Right Occipital
Number of Subjects	10	7	6	8	6	7	5

4.2.3.1 Cross-Subject Power Spectra Results

According to the single-subject results shown in previous sections, we had demonstrated that the motor component was the dominant component to the deviation task, and the frontal component was the dominant component to the math task. Thus the cross-subject EEG power spectra related to different cases in these two components were calculated to show the consistency of our result.

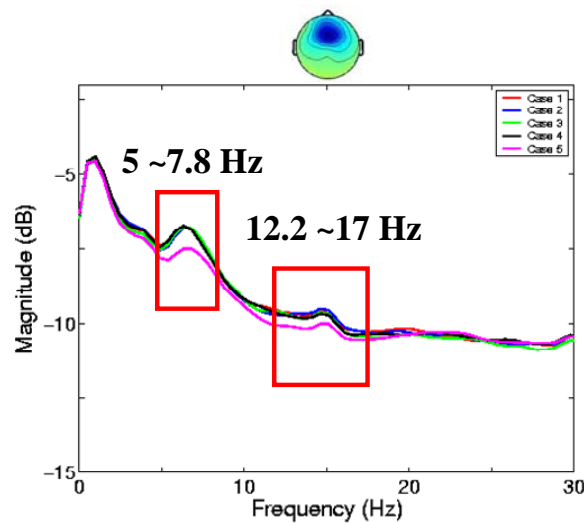
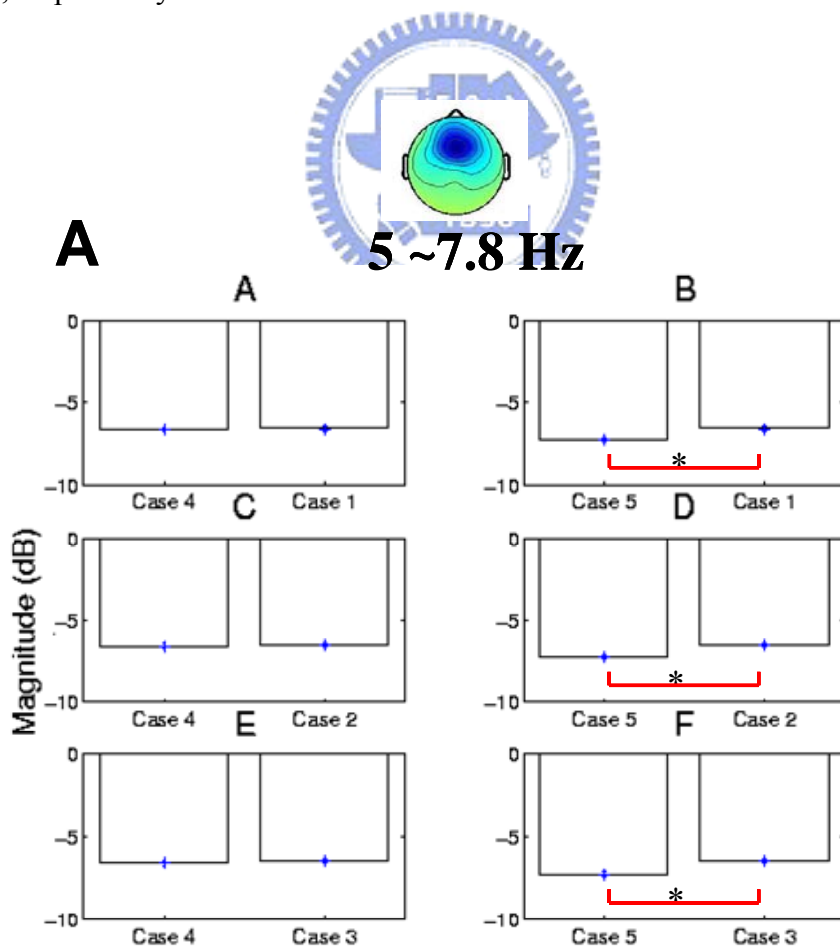


Fig. 4-18: The grand mean of total power spectra for epochs from five cases in the frontal cluster across 10 subjects. The upper panel: the averaged scalp maps for the frontal component across 10 subjects. Red line: case-1, blue line: case-2, green line: case-3, black line: case-4, pink line: case-5. Note: Comparing with the single task, power spectral traces for epochs from dual tasks showed statistically significant increases around theta (5~7.8Hz) and beta (12.2~17Hz) bands.

The grand mean of total power spectra for epochs from five cases in the frontal cluster across 10 subjects were shown in Fig. 4-18. Comparing with the single task, power spectral traces for epochs from dual tasks showed statistically significant increases around theta (5~7.8Hz) and beta (12.2~17Hz) bands. The significance of the differences in 5 ~ 7.8 Hz and 12.2 ~ 17 Hz were tested and shown in Fig. 4-19 (A) and (B), respectively.



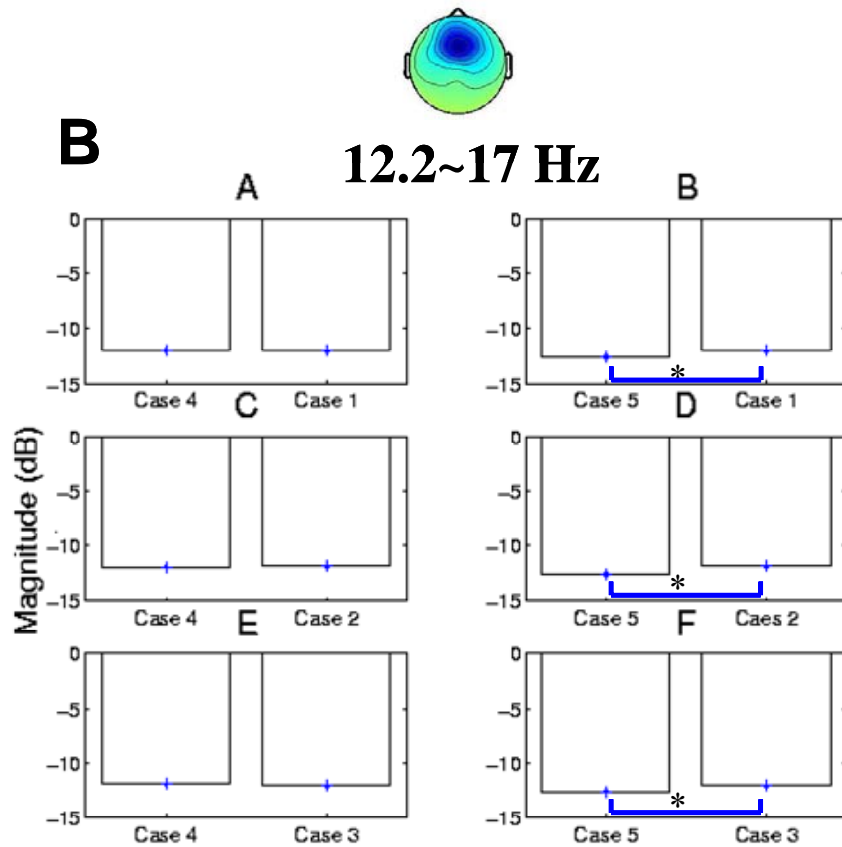


Fig. 4-19: The comparison of the averaged power around the 5~7.8 Hz and 12.2~17 Hz between the single task and dual tasks across 10 subjects in the frontal component. Left column (A, C, E): statistic test between dual-task cases and single math. Right column (B, D, F): statistic test between dual-task cases and single deviation. The upper panel: the averaged scalp maps of the frontal component across 10 subjects. Note: comparing with the single math task, the power around the theta and beta bands were significantly decreased in the dual tasks ($p < 0.01$).

The result of statistic test in frontal cluster was shown in Fig. 4-19. Fig. 4-19 (A) and (B) were showed respectively the statistic test in 5~7.8 Hz and 12.2~17 Hz band between dual-task cases and single case. We had demonstrated that the difference between the single-deviation and the dual-task cases we observed in single subject were also significant in cross-subject results.

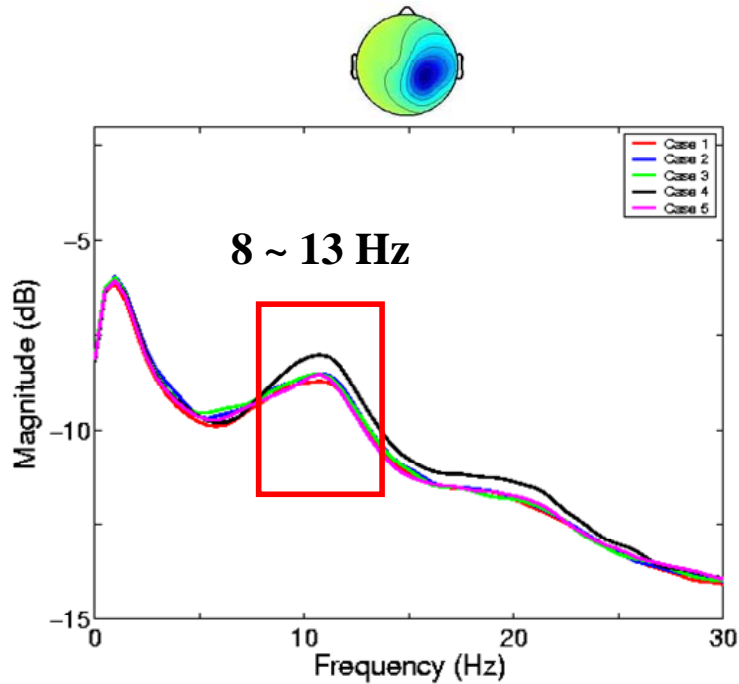


Fig. 4-20: The grand mean of the total power spectra for epochs from five different cases in the right motor cluster across 6 subjects. Panels as Fig. 4-18. Note: comparing with other cases, The power spectral trace for epochs from case-4 showed significantly increased around alpha (8~13Hz) band.

The cross-subject ICA power spectra in the right motor cluster corresponding to the five cases were shown in Fig. 4-20. Significant power differences in alpha band were observed between cases.

Fig. 4-21 was showed the statistic test in 8~13 Hz band between dual-task cases and single case. As shown in Fig. 4-21, the difference between single-math and the dual-task cases were significant. However, the difference between single-deviation and the dual-task cases were also significant in the testing results. According to the statistic results shown in Fig. 4-21, we had demonstrated that the difference between the single-task and the dual-task cases we observed in single subject were also significant in cross-subject results. Thus, we understood the frequency response in motor area was not only influenced by the deviation task but also the math task with pressing a button.

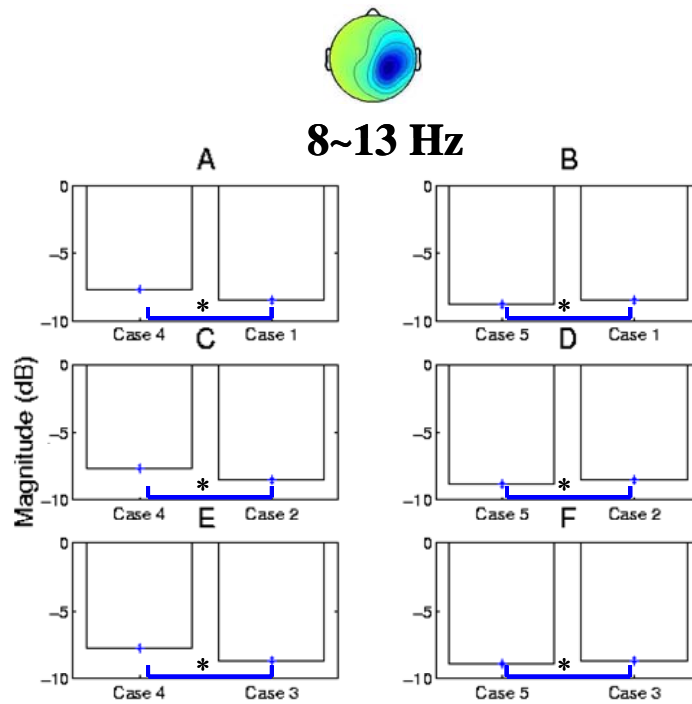


Fig. 4-21: The comparison of the averaged alpha power between the single tasks and dual tasks in the motor cluster. Left column (A, C, E): statistic test between dual-task cases and single math. Right column (B, D, F): statistic test between dual-task cases and single deviation. Note: the frequency response in motor area near the alpha band was not only influenced by the deviation task but also varied by button press.

4.2.3.2 Cross-Subject ERSP Results

The cross-subject averaged ERSP in the frontal cluster corresponding to the five cases were shown in Fig. 4-22. Significant power increases related to the math-task were observed in Fig. 4-22 (A), (B), (C) and (D).

We again demonstrated that the power increase in the frontal cluster is related to math-task. The theta power increase in the three dual-cases including case-1, case-2 and case-3 were slightly different to each other. Comparing to single-math task (Fig.

4-22 (A)), the power in dual-task cases were stronger. EEG theta increase was related to distracted effects in the literatures. Therefore, subjects distracted highest in the case which math presented at 400ms before deviation. The beta power increase which induced by mathematical equations in the literatures was appeared in the math-task and time-locked to mathematics onsets.

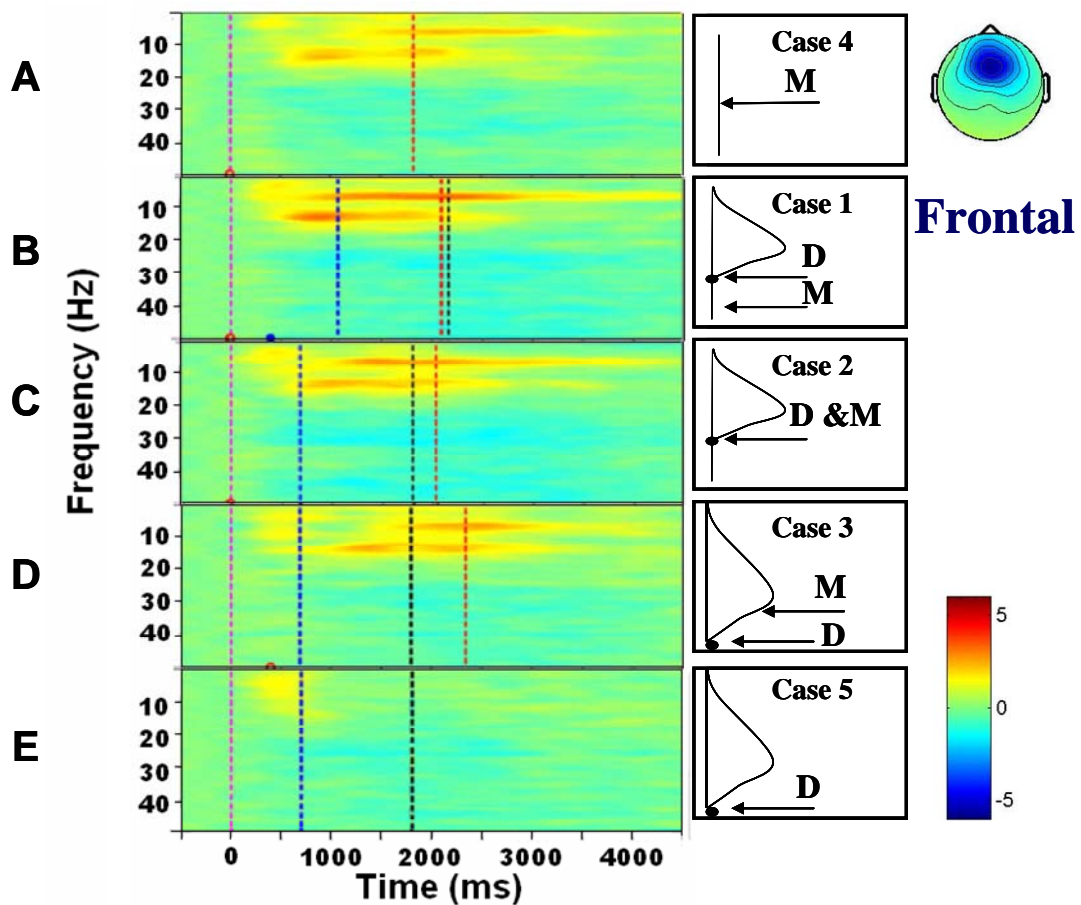


Fig. 4-22: The ERSP images of frontal cluster for five cases: case-4 (A), case-1 (B), case-2 (C), case-3 (D) and case-5 (E). The right column: the averaged scalp maps for the frontal component across 10 subjects. Color bars showed the magnitude of ERSPs. The middle column showed the onset sequences between two tasks. Pink dashed lines: the first event onset. Blue dashed lines: the mean of reaction time to deviation. Red dashed lines: the mean of reaction time to math. Black dashed lines: the averaged response time for car returning to the third lane. Red dot: the onset of math occurred. Blue dot: the onset of deviation presented. Note: the theta (5~7.8 Hz) and beta (12.2~17Hz) power were increased briefly after the math onset. The strongest power increase was observed in case-1. The shortest latency of theta band increase was appeared in case-1.

The comparison of the total power in the four cases with math-task was given in Fig. 4-23, which suggested that the amount of power increase in 5~7.8 Hz were different with different time of SOA. The most significant power increase occurred in case-1.

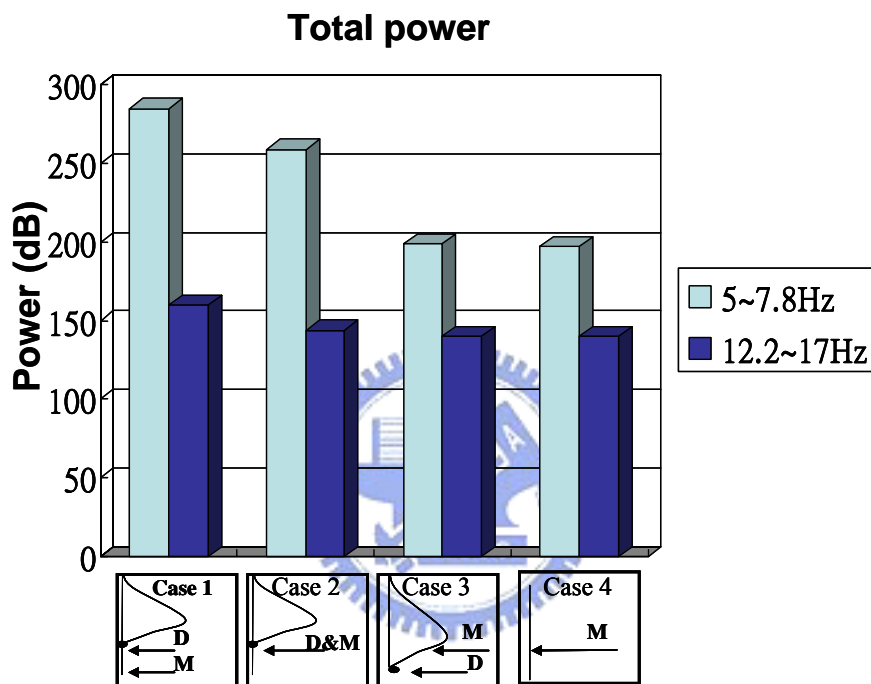


Fig. 4-23: The comparison of total power in cross-subject averaged ERSP images in frontal component between cases. The light blue bar were represented the total power in the theta (5~7.8 Hz) band. The dark blue bars were represented the total power in the beta (12.2~17 Hz) band. The bottom insets showed the onset sequences between two tasks. Note: the most significant power increase was occurred in case-1.

The comparison of the latency of ERSP time-locked to math onsets in the four cases with math-task was given in Fig. 4-24, which suggested that the latency of power increase in 5~7.8 Hz were different with different time of SOA. The shortest latency of power increase occurred in case-1 and the longest latency of power increase occurred in case-4.

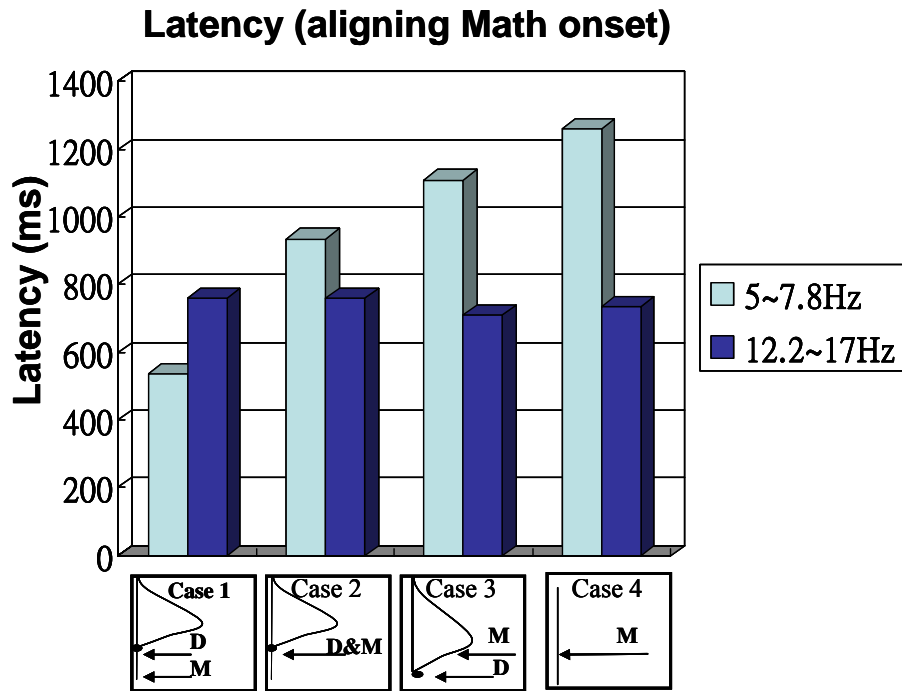


Fig. 4-24: Effects of distraction on onsets of theta and beta increases. Latencies were calculated from cross-subject averaged ERSP images of the frontal component. Panel as Fig. 4-23. Note: the shortest latency of the theta increase was observed in case-1 and the longest latency of the theta increase was revealed in case-4.

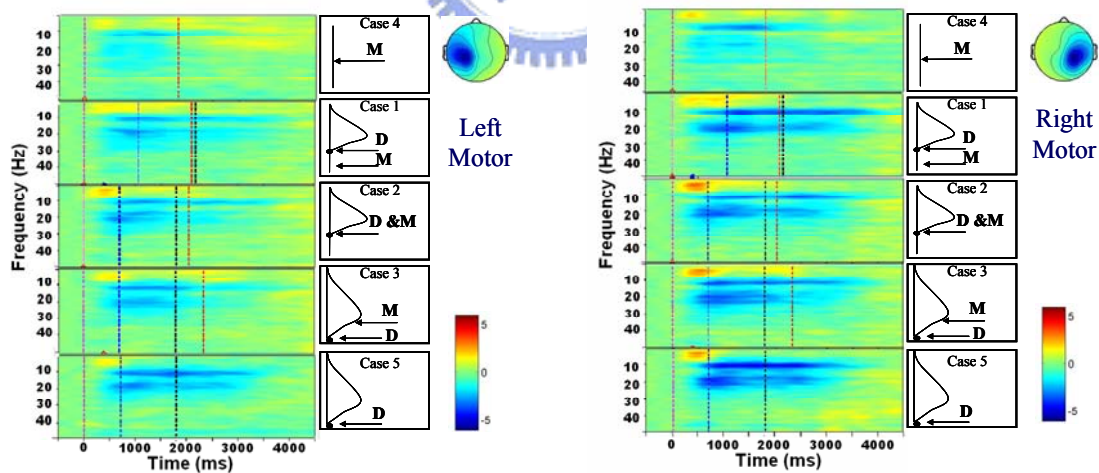


Fig. 4-25: The grand mean of cross-subject averaged ERSP images in left (left block: 8 subjects) and right (right block: 6 subjects) motor components between cases. Left block: left motor cluster. Right block: right motor cluster. Panels as Fig. 4-22. Note: the alpha power was suppressed briefly after the first event onsets in all cases and the strongest alpha suppression was occurred in case-5.

The cross-subject average ERSP in the left and right motor clusters corresponding to the five cases were shown in Fig. 4-25. Significant power suppressions time-locked to event onsets were observed (case-1, case-2, case-3, case-4, and case-5). In case-4, the alpha suppression was observed continuously until the red dashed lines which were the subject response to the event with pressing a button. The alpha suppression continued after the black dashed lines (including case-1, case-2, case-3, and case-5), it maybe control the steering wheel again in the third lane for subjects.

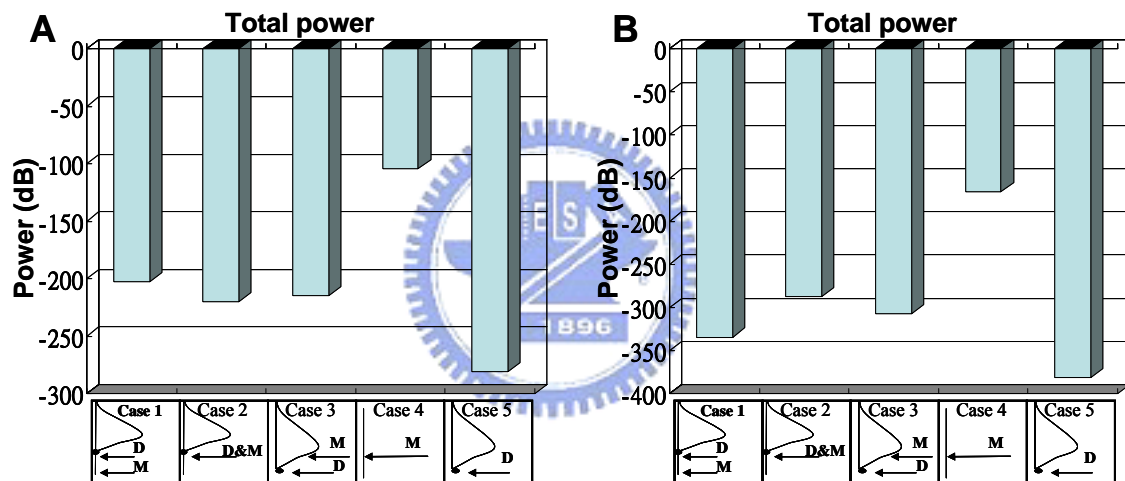


Fig. 4-26: The comparison of total power in cross-subject averaged ERSP images in the left (left block: 8 subjects) and the right (right block: 6 subjects) motor components between cases. The light blue bars represented the total power of the alpha (8~13 Hz) band in individual cases. Note: the most significant power increases were occurred in case-5.

The comparison of the total power in the five cases was given in Fig. 4-26, which suggested that the amounts of power increase in alpha band were different with different time of SOA. The most significant power increase occurred in case-5 (the single-deviation task) and the smallest power increase occurred in case-4 (the single-math task).

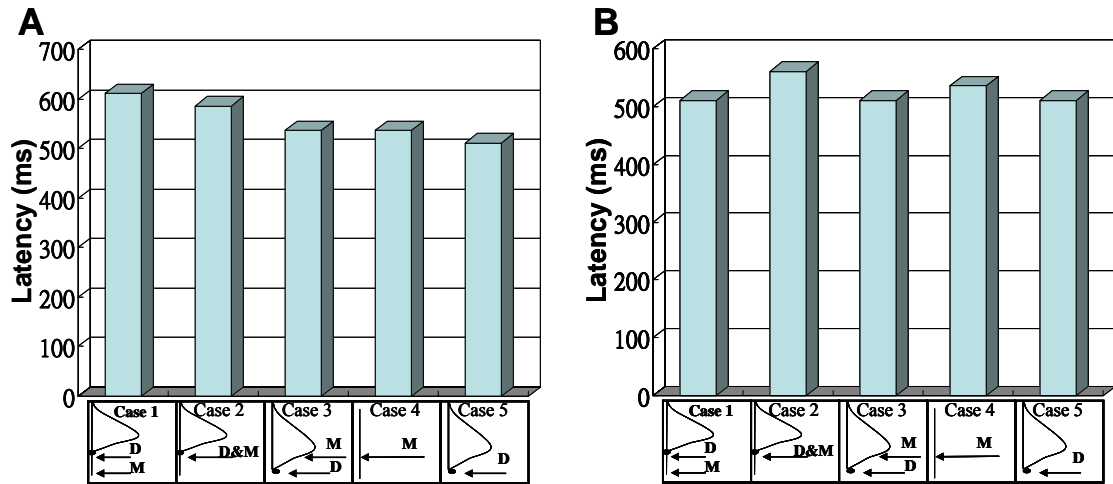


Fig. 4-27: The distracted effects on latencies of alpha suppression measured averaged ERSP images of the motor components. A: the latency of alpha suppression in the left motor cluster across 8 subjects. B: the latency of alpha suppression in the right motor cluster across 6 subjects. Note: no apparently differences were observed among the five cases.

The comparison of the latency of ERSP time-lock to deviation-onset in the five cases was given in Fig. 4-27, which suggested that the latency of power increase in alpha band were not different with different time of SOA. The latency of power increase was following with the event onsets in both right and motor component.

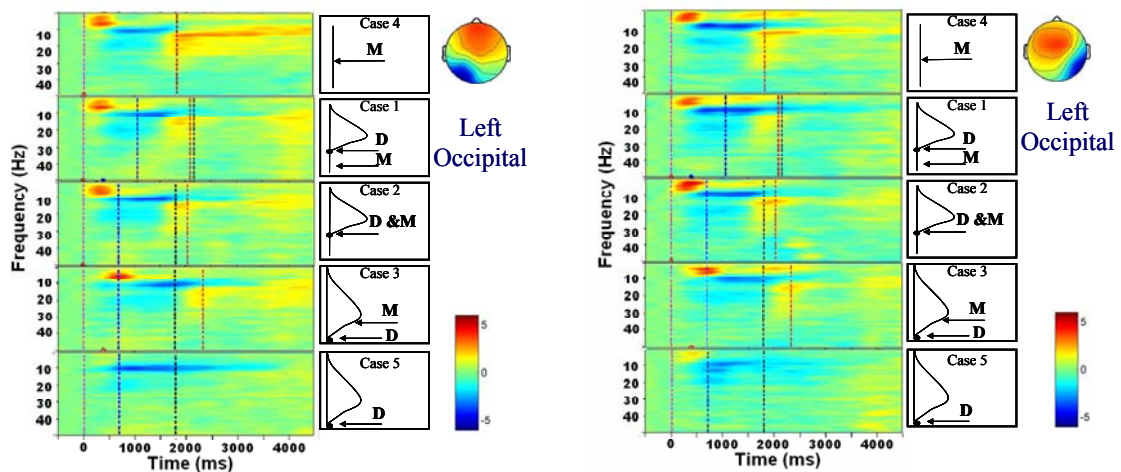


Fig. 4-28: The grand mean of averaged ERSP images of the left (left block: 7 subjects) and right (right block: 5 subjects) occipital clusters for five cases. Panels as Fig. 4-22. Note: the power at lower frequencies (0~8 Hz) was increased briefly after the onsets of the math presented. The most significant alpha power increase was occurred in case-4.

Since the experiment was using visual stimulus, then we could find the pattern inducing by visual stimulus (as shown in Fig. 4-28). In the occipital cluster, we found the lower frequency power which was increase time-locked to math onsets and the most significant alpha power increase which called rebound occurred in case-4. The lower frequency power was induced by P300 (event-related Potential (ERP)) amplitude, as shown in Fig. 4-29.

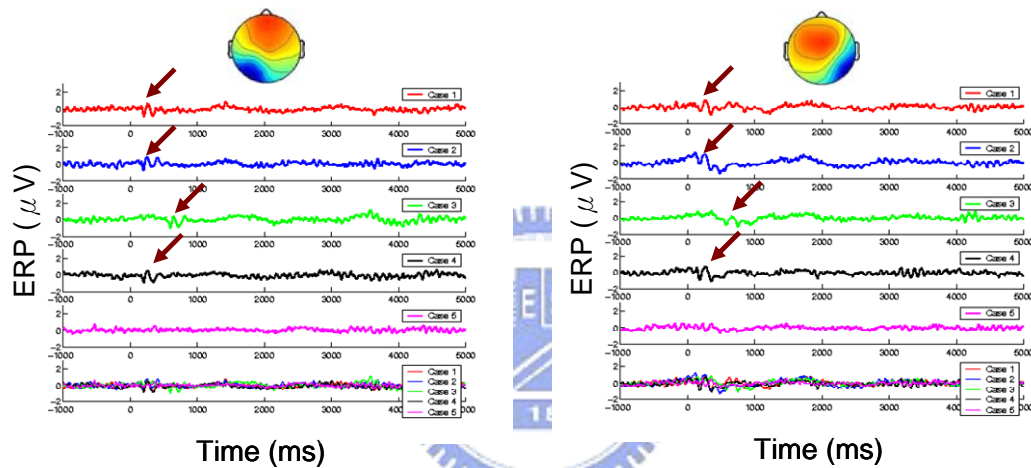


Fig. 4-29: The averaged ERPs of the left (left block: 7 subjects) and right (right block: 5 subjects) occipital clusters for five cases. Upper panels: the group averaged occipital independent component. Red line: case-1, blue line: case-2, green line: case-3, black line: case-4, pink line: case-5. The bottom panels showed all ERP traces. The brown arrows indicated the location of the P300. Note the peak of P300 was time-locked to the onset of math presented.

Our results showed that independent component processes in the frontal cortex exhibited theta (5~7.8 Hz) and beta (12.2~17 Hz) increase that were consistent within subjects. Compared dual-task to single task, the total power in theta (5 ~ 7.8 Hz) band of dual-task was higher than single task. Similarly, the case which presented at 400ms before deviation was highest than that of the other dual-task cases. There was a time sifting at the onset of theta increase in the cases with math events. The beta (12.2~17

Hz) increase was induced by math. In occipital component, we found the pattern of inducing by visual stimulus and rebound which induced by pressing a button. In motor component there was all alpha suppression time-locked to the event onsets.



V. Discussion

In the study, the brain dynamics related to distracted effects of stimulus onset asynchrony (SOA) by using EEG and VR-based realistic driving environment was investigated. The SOA experimental design was to investigate the distracted level. In this Chapter, the results after cross-subject analysis would be discussed. Cross-subject analysis was able to prove that the appeared features were not restricted to specific subject or experiment, that was, it could ensure the stability and consistency of our findings. Firstly, three main cortical areas including frontal component, (which involved processing of mental tasks), somatosensory component (mu suppression phenomenon), and occipital component (the visual-induced and rebound-induced pattern) would be discussed. These cortical areas which had the difference between single and dual-task case would be selected to infer the relationship to the distraction effect and extent. Different frequency band in three cortical areas would also be analyzed. Secondly, we would compare to other literatures of dual-task experiments. Finally, we would discuss the correlation between behavior and EEG. The results would be detailed discussed in the following sections.

5.1 Brain Dynamics Related to Distracted Effect

5.1.1 Distracted Effect in Frontal Area

Frontal lobes are positioned in front of (anterior to) the parietal lobes (as showed in Fig. 5-1). The frontal lobes have been found in response to impulse control, judgment, language production, working memory, motor function, problem solving.

The reports of study were showed divided attention in frontal lobes [46] [47].

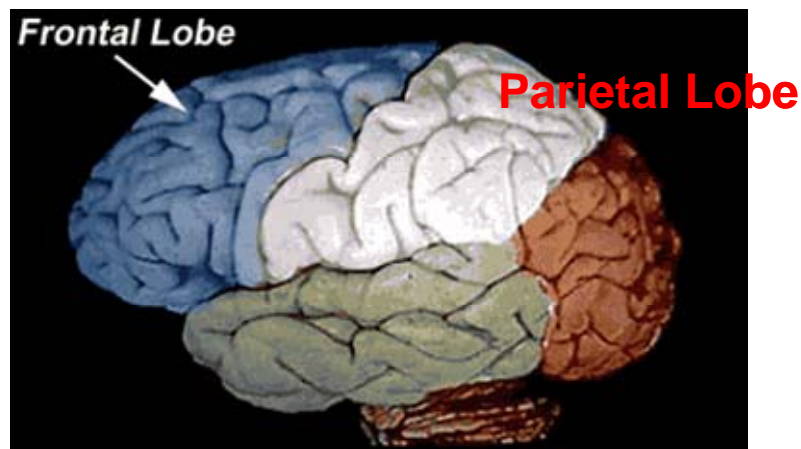


Fig. 5-1: Picture showed the principle fissures and lobes cerebrum [55]. The blue part is the frontal lobe and the white area is the location of parietal lobe.

Fig. 4-23 showed the EEG response (ERSP) in the frontal component under 5 conditions. Compared with the ERS of single task (case-4 and -5), there were higher total power in theta (5 ~7.8 Hz) band of dual tasks (case-1, -2, and -3). The phenomenon suggested that the dual tasks induced more event-related EEG activity in theta band, that was, subjects needed to consume more brain source to accomplish dual tasks at the same time. In a verbal n-back working memory paradigm, evoked theta activity (4-8 Hz) phase-locked to the visual stimulus was evidence in the parieto-occipital and frontal regions in all tasks. It is suggested that theta activity of EEG in the frontal area appears during concentrated performance of mental tasks in normal subjects and reflects attention processing [15]. During mental work load, the EEG process producing 5-7 Hz frontal midline theta activity. The process accounting for the EEG theta increase in midline frontal area during mental work load was separated from channel data into independent brain sources by ICA [45]. Therefore, the theta band increase together with the raising workload is associated with numerous processes such as mental work load, solving problem, encoding, or self

monitoring.

According to the evidences presented in previous studies, we could first prove that the subjects were distracted under dual-task conditions in the experiment. Furthermore, we would like to compare the differences in specific bands among the three kinds of dual-task conditions, as shown in Fig. 4-24.

Compared with total power intensity among dual-task conditions, the total power of math-before-400ms was higher than that of the other dual-task cases. It was suggested that the maximal energy will be induced when the second task present following the other task is current under processing. In addition, since human visual sensory needs about at 300 ms to perceive stimulus (P300 activity [48]), 400 ms is sufficient for subject to process the first task. There was a processing task in brain first and subjects needed more brain source to manage the second task presented after the first task at 400 ms. Therefore, the total power in theta (5~7.8 Hz) band of math-400ms-deviation case was higher than that of the other dual-task cases. In the case of deviation-400ms-math, subjects just dealt with the simple deviation task first, and then processed the task of math. The theta power in deviaiton-400ms-math case was not higher than that of math-400ms-deviaiton case. The other fact was the onset of significant theta power presented, as shown in Fig. 4-24. It was clearly that the theta power increase presented most early in math-400ms-deviation than that in the other cases. The early phyasic theta band response in frontal regions primarily reflected the activation of neural networks involved in allocation of attention related to target stimulus [49].

We also found power increase in beta band (12.2 ~ 17 Hz) in all cases (as showed in Fig. 4-22). From the ERSP images, the patterns were time-locked to the onsets of the math. It is suggested that EEG changed due to a specific component of mental calculation. Significant differences were obtained in delta and theta band in

right posterior areas and in the beta band in frontal areas [50].

The presented evidence proved that when human faced a difficult task first and then the other tasks presented, it would not only be induced the faster attention-related activation, but also led to the maximal distraction effect in the experiment. The theta activity of EEG in the frontal area could be used as the index of distracted effect and distracted extent.

5.1.2 Distracted Effect in Mu Area

Mu rhythm (μ rhythm) is an EEG rhythm recorded usually from the motor cortex of the dominant hemisphere. It is also called aciform rhythm given the shape of the waveforms. It is a variant of normality, and it can be suppressed by a simple motor activity such as clenching the fist of the contra lateral side, or passively moved [51] [52] [53]. Mu suppression is believed to be the electrical output of the synchronization of large portions of pyramidal neurons of the motor cortex which control the hand and arm movement when it is inactive.

According to the ERSP of single deviation and single math in Fig. 4-25, respectively, the mu suppression was caused mostly by subjects steering the wheel and pressing the bottoms (answer mathematical questions). It was obviously that the mu suppression caused by wheel steering is almost time-locked to the response onset. The mu suppression caused by bottom press was present before the math reply. Suggest that it involves motor planning to prepare to answer the math question [54]. As for in the dual-task cases, the mu suppression was mixed by the two main reasons, wheel steering and bottom press, and it was weaker in dual -task cases than that in single-task. Due to the more activation in dual-task cases in the frontal lobe, it may be

reasonable to infer that the math processing occupy more brain source in frontal lobe so that the less activation was induced in the motor area. However, it was difficult to find an index of distraction effect and distraction extent in motor area since the mixed/undistinguishable activity.

5.1.3 Distracted Effect in Occipital Area

The occipital lobe is the visual processing center of the mammalian brain, containing most of the anatomical region of the visual cortex. The region specialized for different visual tasks, such as visuospatial processing, color discrimination and motion perception [55].

In our experiment, we also investigated the pattern inducing by visual stimulus. In Fig. 4-28, power increase in low frequency accompanied the onset of math. From the ERP (Fig. 4-29) activity, we also found the pattern of P300 that involves the visual induced activity [56]. According to ERSF of the single math case, the alpha increase was time-locked to the response of math reply. The phenomenon is known as alpha rebound after a mental task being finished [57]. Compared with other cases with math, the alpha rebound power was maximal in the single math case. It is suggested that the subjects were able to concentrate on solving math task without other distraction in the single-math case. It is also suggested that perceptual switching by the button press showed characteristic occipital alpha and frontal theta band activity prior to a switch [59]. The alpha activity was specific to switch, the theta activity was generic to perceptual processing conditions. These results suggest that the ability to concentrate attentional effort on the task is responsible for the differences in perceptual switching rates.

5.2 Brain Dynamics Related to Dual Task

Of particular importance here, was the observation that interaction elicited by two visual stimulus. In the literature, subjects viewed the Necker cube continuously and responded perceptual switching by pressing a button. It suggests that the ability to concentrate attentional effort on the task is responsible for the difference in perceptual switching rate [58]. For selective multi objects, human attention requires that its object be selected from among others, and that the representation of the selective object be effectively integrated with information in other brain areas mediating higher cognitive processing. It demonstrates that the main role of cognitive processing in the brain is in selective attention when subjects select object to act [59]. Similarly, in dual-task coordination, subjects increased distracted interference in selective attention. Posner et al. [60] postulated that two tasks, when performed simultaneously, do not interfere with the performance of one another when different brain areas are used for the two tasks. Brain activation during simultaneous visual and auditory information processing may result in a summation of the activation during selective visual and auditory information processing (selective or focused attention). One report is to investigate how performance of two overlapping discrete tasks is organized and controlled. It suggests that sequential performance of overlapping tasks is scheduled in advance and is regulated by initially allocating the central processing channel to one task and subsequently switching this channel to the other task [61].

In our experiment, because we used two visual stimuli and they would compete within the same brain source to interfere with the performance of one another. From the results, the phasic changes around the theta band for the case, which the math presented at 400ms before the deviation onset, showed the highest distracted effect in

all cases, not two tasks appeared simultaneously. Then, we inferred that when math task was presented to the subject, it occupied most of the brain source. Thus when deviation task appeared the brain immediately allocated to switch to the second task and the influence would consume many brain sources.

In the case which deviation presented at 400ms before math, since the design of the deviation task was very simple in our experiment, thus when the deviation was presented to the subject, it did not consume much brain source. Therefore, when the second (the math) task appeared the brain could immediately allocate source to switch the task.

Similarly, when two tasks were presented simultaneously to the subject, the subject would select an important task from the two tasks and replied to the task immediately. And thus, brain could easily allocate source to switch next task, because brain had organized the operating sequence.

In summary, we investigated the relationship between brains activities associated with dual-task management and the combination of response modalities and observed several differences in neural activities between dual-task cases and single case.

5.3 The Correlation between Behavioral and Physiological Responses

In our experiment, we found that the phenomena of trend of response time (math) and EEG theta increase in frontal lobe were consistency. The response time of math was the shortest and the EEG theta power increase was the weakest in the case of single math. Similarly, in the case of case-1 there was the longest of response time of math and the strongest total power (as shown in Fig. 4-23 and Fig. 4-24).

In the study, the deviation task was much easier than the math task. Therefore, this would affect the distraction according to the sequence of two tasks. According to the observation of on-board camera video during driving experiment, it was found that most subjects took the math as a cue and turned rapidly in the case of math-400ms-deviation. And when the deviation task appeared in the case-1 subjects were in order to continuously resolve the mathematical equations, they had to firstly and rapidly response to the deviation task to avoid hitting the wall. Therefore, we found that the response time was the shortest in the case of math-400ms-deviation, but the longest time in the case of single-deviation. In motor component, the alpha suppression was weaker in the dual-task cases than that in the case of single-deviation. The trend between response time of deviation and alpha suppression in motor area was not consistency. This was due to our designed experiment. To avoid the problem presented, we could adjust some parameters in next experiment. Firstly, we had to increase the degree of difficulty about deviation. When a winding course added the experiment, subjects consumed more force in driving. Secondly, we could control to be not the same as the ratio of appearing cases and in order to simulate real driving, we designed higher rate in single deviation similar to oddball paradigm. This was in order to investigate that the second task affected the primarily task of driving.

VI. Conclusions

To investigate the brain dynamics related to distracted effects by using EEG signals, we assessed effects of the stimulus onset asynchrony (SOA) between the deviation and math presented on the EEG dynamics and we designed five cases with different SOA. This innovative study was conducted in a VR-environment on a 6 DOF motion platform. Our results showed that behavioral and physiological (EEG) responses under multiple cases and multiple distracted levels include: (1) Behavior: the statistic test of response time to math in dual tasks was significantly larger than that in single task and the response time of single-math was shortest. This was because there was no another task to interference. However, comparing to the dual tasks, the response time to deviation was longest in the case of single-deviation. This was because the math task of the designed is difficult enough for the subjects and was considered as a real cue in the experiment. (2) Frontal component: (a) comparing to the single tasks, the phasic theta (5~7.8 Hz) band increase was higher in dual tasks. The phasic changes around the theta band for the case, which the math presented at 400ms before the deviation onset, showed the strongest increases among all dual-task cases. (b) The latencies of the theta increase were shifted along with the onset of math presented. The latency for the case which the math presented at 400ms before deviation appeared was the shortest. (c) The Beta (12.2 ~ 17 Hz) increase was induced by the onsets of the math. (3) Motor component: alpha suppressions were time-locked to onsets of the first event. (4) Occipital component: (a) ERPs time-locked to the onsets of the math were showed in all cases. In comparison with the single task, the rebounded activities near the alpha band that induced by the button press were significantly decreased in the dual tasks.

When received a dual-task performance, subjects made math as a cue, and they could steer wheel rapidly. Comparing to among dual-task cases, the phasic theta band increases was higher in dual tasks. The phasic changes around the theta band for the case, which the math presented at 400ms before the deviation onset, showed the highest distracted effect in all cases. Because there was a processing task in brain first and subjects needed more brain source to manage the second task presented after the first task at 400 Ms. As for in the dual-task cases, less alpha suppression was in motor area, but more theta increase was in frontal area. These results demonstrated that reaction time and multiple cortical EEG sources responded to the car drifting and the math occurrences differentially in the stimulus onset asynchrony. In addition, results also suggested that the phasic theta increase in frontal area could be used as the index for early detecting driver's distraction in the real driving.

In the future, firstly, we will apply our finding to take one step ahead to investigate the difference about spatial attention between motion and motionless on a 6 DOF motion platform. Secondary, in order to simulate real driving, we can investigate multi-sensory attention (such as auditory and visual). We will further investigate more detailed about the distracted effects of stimulus onset asynchrony. In the future, we use the study to combine the mechanism of bio-feedback and the bio-feedback provides a warning for the brain to adapt when subjects distract.

Reference

- [1] J.C. Stutts, D.W. Reinfurt, L. Staplin, and E.A. Rodgman, "The role driver distraction in traffic crashes," *AAA Foundation for Traffic Safety*, 202, 638-5944, 2003.
<http://www.aaafoundation.org/pdf/distraction.pdf>
- [2] T. Horberry, J. Horberry, M.A. Anderson, T. Regan, J. Triggs, and J. Brown, "Driver distraction: the effects of concurrent in-vehicle tasks, road environment complexity and age on driving performance," *Accident Analysis & Prevention*, 38, 185-191, 2006.
- [3] C.J.D. Patten, J. Kircher, L. Östlund, and L. Nilsson, "Using mobile telephones: cognitive workload and attention resource allocation," *Accident Analysis & Prevention*, 36, 341-350, 2004.
- [4] T. Dukic, L. Hanson, and T. Falkmer, "Effect of drivers' age and push button locations on visual time off road, steering wheel deviation and safety perception," *Ergonomics*, 49, 78-92, 2006.
- [5] J.D. Lee, B. Caven, S. Haake, and T.L. Brown, "Speech-based interaction with in-vehicle computers: the effect of speech-based e-mail on drivers' attention to the roadway," *Humam Factors*. 43, 631-640, 2001.
- [6] L. Tijerina, S. Johnston, and E. Parmer, Winterbottom, M.D., Goodman, M. "Driver Distraction with Route Guidance Systems Report No DOT HS 809-069," *National Highway Traffic Safety Administration*, 2000.
- [7] P. A. Hancock, M. Lesch, and L. Simmons, "The distraction effects of phone use during a crucial driving maneuver," *Accident Analysis & Prevention*, 35, 501-541, 2003.
- [8] D.L. Sraayer, F.A. Drews, and W.A. Johnston, "Cell phone-Induced Failures of Visual Attention During Simulated Driving," *Journal of Experimental*

Psychology, 9, 23-32 ,2003.

- [9] R. W. Hahn, P. C. Tetlock, and J. K. Burnett, "Should You Be Allowed to Use Your Cellular phone while Driving?," *Regulation*, 23, 46-55, 2000.
- [10] D. Crundall, E. Crundall, V. Loon, and G. Underwood, "Attraction and distraction of attention with roadside advertisements," *Accident Analysis & Prevention*, 38, 671-677, 2006.
- [11] S. Amado, S. Ulupinar, P. Amado, and P. Ulupinar, "The effects of conversation on attention and peripheral detection: is talking with a passenger and talking on the cell phone different?," *Transportation Research*, 8, 383-395, 2005.
- [12] D.J. Madden, T.G. Turkington, J.M. Provenzale, J.M. Hawk, T.C. Hoffman, and R.E. Coleman, "Selective and divided visual attention: Age-related changes in regional cerebral blood flow measured by H215O PET," *Human Brain Mapping*, 5,389-409, 1997.
- [13] M. Corbetta, F.M. Miezin, S. Dobmeyer, G.L. Shulman, and SE. Petersen, "Selective and divided attention during visual discriminations of shape, color, and speed: functional anatomy by positron emission tomography," *J Neuroscience*, 11, 2383-2402 , 1991.
- [14] E. Koechlin, G. Basso, P. Pietrini, S. Panzer, and J. Grafman, "The role of the anterior prefrontal cortex in human cognition," *Nature*, 399, 148 -151, 1999.
- [15] M.P. Deiber, P. Missonnier, O. Bertrand, G. Gold, L. Fazio-Costa, V. Ibañez, and P. Giannakopoulos, "Distinction between Perceptual and Attentional Processing in Working Memory Tasks: A Study of Phase-locked and Induced Oscillatory Brain Dynamics," *Journal of Cognitive Neuroscience*, 19, 158-172, 2007.
- [16] A. J. Szameitat, J. Lepsien, D. Y. Cramon, A. Sterr, and T. Schubert, "Task-order coordination in dual-task performance and the lateral prefrontal cortex: an event related fMRI study," *Psychological Research*, 2, 1-12, 2006.
- [17] C. Stelzel, E. H. Schumacher, T. Schubert, and M. D'Esposito, "The neural effect

of stimulus-response modality compatibility on dual-task performance: an fMRI study,” *Psychological Research*, 70, 514-525, 2005.

[18] L. Carryl, L. Baldwin, L. Joseph, and T. Coyne, “Mental workload as a function of traffic density: Comparison of physiological, behavioral, and subjective indices,” *Proceedings of the Second International Driving Symposium on Human Factors in Driver Assessment, Training and Vehicle Design*, 2003.

[19] M.E. Rakauskas, N.J. Ward, E.M. Bernat, M. Cadwallader, C.J. Patrick, and D. de Waard, “Psychophysiological measures of driver distraction and workload while intoxicated,” *International Symposium on Human Factors in Driver Assessment, Training, and Vehicle Design*. 6, 27-30, 2005.

[20] C.T. Lin, C.R. Wu, S.F. Liang, T.Y. Huang, W.H. Chao, Y.J. Chen, and T.P. Jung, “EEG-based Drowsiness estimation for safety driving using independent component analysis,” *IEEE Transactions on Circuit and System*, 52, 2726-2738, 2005.

[21] H. J. Eoh, M. K. Chung, and S. H. Kim, “Electroencephalographic study of drowsiness in simulated driving with sleep deprivation,” *International Journal of Industrial Ergonomics*, 35, 307-320, 2005.

[22] A. Kemeny, and F. Panerai, “Evaluating perception in driving simulation experiments,” *TRENDS in Cognitive Sciences*, 7, 31-37, 2003.

[23] C.T. Lin, R.C. Wu, T.P. Jung, S.F. Liang, and T.Y. Huang, “Estimating Driving Performance Based on EEG Spectrum Analysis,” *EURASIP Journal on Applied Signal Processing*, 19, 3165-3174, 2005.

[24] UW Computing & Communications

URL: <http://faculty.washington.edu/chudler/1020.html>

[25] S. Makeig, A. Bell, T.P. Jung, and T. Sejnowski, “Independent component analysis of electroencephalographic data,” *Advance in Neural Information Processing System*, 8, 145-151, 1995.

- [26] C. Jutten, and J. Herault, "Blind separation of sources I. an adaptive algorithm based on neuromimetic architecture," *Signal Process*, 24, 1-10, 1991.
- [27] J.F. Cardoso, and A. Souloumiac, "Blind beamforming for non Gaussian signals," *IEEE Proceedings-F 140*, 6, 362-370, 1993.
- [28] P. Comon, "Independent component analysis - A new concept," *Signal Processing*, 36, 287-314, 1994.
- [29] A.J. Bell, and T.J. Sejnowski, "An information-maximization approach to blind separation and blind deconvolution," *Neural Computation*, 7, 1129-1159, 1995.
- [30] J.F. Cardoso, and B. Laheld, "Equivariant adaptive source separation," *IEEE Transactions on Signal Processing*, 45, 434-444, 1996.
- [31] D.T. Pham, "Blind separation of instantaneous mixture of sources via an independent component analysis," *IEEE Transactions on Signal Processing*, 44, 2768-2779, 1997.
- [32] M. Girolami, "An alternative perspective on adaptive independent component analysis," *Neural Computation*, 10, 2103-2114, 1998.
- [33] T.W. Lee, M. Girolami, and T.J. Sejnowski, "Independent component analysis using an extended infomax algorithm for mixed sub-Gaussian and super-Gaussian sources," *Neural Computation*, 11, 606-633, 1999.
- [34] S. Makeig, A.J. Bell, T.P. Jung, and T.J. Sejnowski, "Independent component analysis of Electroencephalographic data," *Advances in Neural Information Processing Systems* 8, 145-151, 1996.
- [35] T.P. Jung, C. Humphries, T.W. Lee, S. Makeig, M.J. McKeown, V. Iragui, and T.J. Sejnowski, "Extended ICA removes artifacts from electroencephalographic recordings," *Advances in Neural Information Processing Systems*, 10, 894-900, 1998.
- [36] T.P. Jung, S. Makeig, C. Humphries, T.W. Lee, M.J. McKeown, V. Iragui, and T.J.

- Sejnowski, "Removing electroencephalographic artifacts by blind source separation," *Psychophysiology*, 37, 163-178, 2000.
- [37] T.P. Jung, S. Makeig, W. Westerfield, J. Townsend, E. Courchesne, and T.J. Sejnowski, "Analysis and visualization of single-trial event-related potentials," *Human Brain Mapping*, 14, 166-185, 2001.
- [38] A. Yamazaki, T. Tajima, and K. Matsuoka, "Convulsive independent component analysis of EEG data," *Annual Conference on SICE*, 2, 1227-1231, 2003.
- [39] A. Meyer-Base, D. Auer, and A. Wismueller, "Topographic independent component analysis for fMRI signal detection," *Proceedings of the International Joint Conference on Neural Networks*, 1, 601-605, 2003.
- [40] M. Naganawa, Y. Kimura, K. Ishii, K. Oda, K. Ishiwata, and A. Matani, "Extraction of a plasma time-activity curve from dynamic brain pet images based on independent component analysis," *IEEE Transactions on Biomedical Engineering*, 52, 201-210, 2005.
- [41] R. Liao, J.L. Krolik, and M.J. McKeown, "An information-theoretic criterion for intrasubject alignment of FMRI time series: motion corrected independent component analysis," *IEEE Transactions on Medical Imaging*, 24, 29-44, 2005.
- [42] S. Makeig, "Auditory event-related dynamics of the EEG spectrum and effects of exposure to tones," *Electroencephalography and Clinical Neurophysiology*, 86, 283-293, 1993.
- [43] S. Makeig, M. Westerfield, T.P. Jung, S. Enghoff, J. Townsend, E. Courchesne, and T.J. Sejnowski, "Dynamic brain sources of visual evoked responses," *Science*, 295, 690-694, 2002.
- [44] S. Makeig, A. Delorme, M. Westerfield, J. Townsend, E. Courchense, and T. Sejnowski, "Electroencephalographic brain dynamics following visual targets requiring manual responses," *PLOS Biology*, 2, 0747, 2004.

- [45] J. Onton, A. Delorme, and S. Makeig, "Frontal Midline theta dynamics during working memory," *Neuroimage*, 27, 341-356, 2005.
<http://www.aaafoundation.org/pdf/distraction.pdf>
- [46] P. W. Burgess, "Strategy Application Disorder: the Role of the Frontal Lobes in Human Multitasking," *Psychophysiology*, 63, 279-288, 2000.
- [47] J. Sarthein, H. Petsche, P. Rappelsberger, G.L. Shaw, and V. Stein, "A Synchronization between prefrontal and posterior association cortex during human working memory," *Proceedings of the National Academy of Sciences of the United States of America*, 95, 7092-7096, 1998.
- [48] SM. Jensen, A. Barabasz, M. Barabasz, and D. Warner, "EEG P300 event-related markers of hypnosis," *clinical hypnosis*, 44, 127-39, 2001.
- [49] P. Missonnier, M.P. Deiber, G. Gold, P. Millet, M. Gex-Fabry, Pun. L. Fazio-Costa, P. Giannakopoulos and V. Ibáñez. "Frontal theta event-related synchronization: comparison of directed attention and working memory load effects," *Journal of Neural Transmission*, 10, 1477-1486, 2006.
- [50] T. Fernández, T. Harmony, M. Rodríguez, J. Bernal, J. Silva, A. Reyes, and E. Marosi, "EEG activation patterns during the performance of tasks involving different components of mental calculation," *Electroencephalogr Clin Neurophysiol*, 94, 175-182, 1995.
- [51] W.N. Kuhlman, "EEG feedback training: enhancement of somatosensory cortical Activity," *Electroencephalogr Clin Neurophysiol*, 45, 290-294, 1978.
- [52] W.N. Kuhlman, "Functional topography of the human Mu rhythm," *Electroencephalogr Clin Neurophysiol*, 44,83-93, 1978.
- [53] M. Schoppenhorst, F. Brauer, G. Freund, and St. Kubichi, "The significance of coherence estimates in determining central alpha and mu activities," *Electroencephalogr Clin Neurophysiol*, 48, 25-33, 1980.

- [54] M. Hayhoe, A. Shrivastava, Jeff B. Pelz. Mruczek, “Visual memory and motor planning in a natural task,” *Journal of Vision*, 6, 49-63, 2003.
- [55] E. Kandel, J. Schwartz, and T. Jessell, “Principles of Neural Science,” 3rd edition.
- [56] J.V. Odom, M. Bach, and C. Barber, “Visual evoked potentials standard,” *Documenta ophthalmologica. Advances in ophthalmology*, 108, 115-123, 2004.
- [57] G. Pfurtscheller, C. Neuper, C. Brunner, and FL. da Silva, “Beta rebound after different types of motor imagery in man,” *Neuroscience Letters*, , 378, 156-159 ,2005.
- [58] H. Nakatani, and C. van Leeuwen, “Individual differences in perceptual switching rates; the role of occipital alpha and frontal theta band activity,” *Biological Cybernetics*, 93, 343-354, 2005.
- [59] N. Lavie, A. Hirst Jan, W. de Fockert, and E. Viding, “Load Theory of Selective Attention and Cognitive Control,” *Journal of Experimental Psychology*, 9, 339-354, 2004.
- [60]MI. Posner, J. Sandson, M. Dhawan, and GL. Shulman, “Is word recognition automatic? A cognitive-anatomical approach,” *Journal of Cognitive Neuroscience*, 1, 50-60, 1989.
- [61]R. De Jong, “The role of preparation in overlapping-task performance,” *Quarterly Journal of Experimental Psychology*, 48, 2-25, 1995.
- [62]S. Makeig, T.P. Jung, and T. J. Sejnowski, “Awareness during drowsiness: dynamics and electrophysiological correlates,” *Canadian Journal of Experimental Psychology*, 54, 266-273, 2000.

Appendix

A. Independent Component Analysis (ICA)

The ICA is a statistical “latent variables” model with generative form:

$$\mathbf{x}(t) = \mathbf{A}s(t) \quad (1)$$

Where \mathbf{A} is a linear transform called a mixing matrix and the s_i are statistically mutually independent. The ICA model describes how the observed data are generated by a process of mixing the components s_i . The independent components s_i (often abbreviated as *ICs*) are latent variables, meaning that they cannot be directly observed. Also the mixing matrix \mathbf{A} is assumed to be unknown. All we observed are the random variables x_i , and we must estimate both the mixing matrix and the *IC*'s s_i using the x_i .

Therefore, given time series of the observed data $\mathbf{x}(t) = [x_1(t) \ x_2(t) \ \cdots \ x_N(t)]^T$ in N -dimension, ICA will find a linear mapping \mathbf{W} such that the unmixed signals $\mathbf{u}(t)$ is statically independent.

$$\mathbf{u}(t) = \mathbf{W} \mathbf{x}(t). \quad (2)$$

Supposed the probability density function of the observations \mathbf{x} can be expressed as:

$$p(\mathbf{x}) = |\det(\mathbf{W})| p(\mathbf{u}), \quad (3)$$

the learning algorithm can be derived using the maximum likelihood formulation with the log-likelihood function derived as:

$$\mathbf{L}(\mathbf{u}, \mathbf{W}) = \log |\det(\mathbf{W})| + \sum_{i=1}^N \log p_i(u_i), \quad (4)$$

Thus, an effective learning algorithm using natural gradient to maximize the

log-likelihood with respect to \mathbf{W} gives:

$$\Delta \mathbf{W} \propto \frac{\partial L(\mathbf{u}, \mathbf{W})}{\partial \mathbf{W}} \mathbf{W}^T \mathbf{W} = [\mathbf{I} - \varphi(\mathbf{u}) \mathbf{u}^T] \mathbf{W}, \quad (5)$$

Where the nonlinearity

$$\varphi(\mathbf{u}) = -\frac{\frac{\partial p(\mathbf{u})}{\partial \mathbf{u}}}{p(\mathbf{u})} = \left[-\frac{\frac{\partial p(u_1)}{\partial u_1}}{p(u_1)} \quad \dots \quad -\frac{\frac{\partial p(u_N)}{\partial u_N}}{p(u_N)} \right]^T, \quad (6)$$

and $\mathbf{W}^T \mathbf{W}$ rescales the gradient, simplifies the learning rule and speeds the convergence considerably. It is difficult to know a priori the parametric density function $p(\mathbf{u})$, which plays an essential role in the learning process. If we choose to approximate the estimated probability density function with an Edgeworth expansion or Gram-Charlier expansion for generalizing the learning rule to sources with either sub- or super-Gaussian distributions, the nonlinearity $\varphi(\mathbf{u})$ can be derived as:

$$\varphi(\mathbf{u}) = \begin{cases} \mathbf{u} - \tanh(\mathbf{u}) & \text{for super - gaussian sources,} \\ \mathbf{u} + \tanh(\mathbf{u}) & \text{for sub - gaussian sources,} \end{cases} \quad (7)$$

Then,

$$\Delta \mathbf{W} = \begin{cases} [\mathbf{I} - \tanh(\mathbf{u}) \mathbf{u}^T - \mathbf{u} \mathbf{u}^T] \mathbf{W} & \text{super - gaussian,} \\ [\mathbf{I} + \tanh(\mathbf{u}) \mathbf{u}^T - \mathbf{u} \mathbf{u}^T] \mathbf{W} & \text{sub - gaussian,} \end{cases} \quad (8)$$

Since there is no general definition for sub- and super-Gaussian sources, we choose

$$p(\mathbf{u}) = \frac{1}{2}(N(1,1) + N(-1,1)) \quad \text{and} \quad p(\mathbf{u}) = N(0,1) \operatorname{sech}^2(\mathbf{u}) \quad \text{for sub- and}$$

super-Gaussian, respectively, where $N(\mu, \sigma^2)$ is a normal distribution. The learning rules differ in the sign before the \tanh function and can be determined using a switching criterion as:

$$\Delta \mathbf{W} \propto [\mathbf{I} - \mathbf{K} \tanh(\mathbf{u}) \mathbf{u}^T - \mathbf{u} \mathbf{u}^T] \mathbf{W}, \quad \text{where} \quad \begin{cases} \kappa_i = 1 & \text{super - gaussian,} \\ \kappa_i = -1 & \text{sub - gaussian,} \end{cases} \quad (9)$$

where

$$\kappa_i = \text{sign}\left(E\{\text{sech}^2(u_i)\}E\{u_i^2\} - E\{\tanh(u_i)u_i\}\right), \quad (10)$$

represents the elements of N -dimensional diagonal matrix \mathbf{K} . After ICA training, we can obtain N ICA components $\mathbf{u}(t)$ decomposed from the measured N -channel EEG data $\mathbf{x}(t)$. In this study, $N=30$, thus we obtain 30 components from 30 channel signals.

$$\mathbf{x}(t) = \begin{bmatrix} x_1(t) \\ x_2(t) \\ \vdots \\ x_{33}(t) \end{bmatrix} = \mathbf{W}\mathbf{u}(t) = \begin{bmatrix} w_{1,1} \\ w_{2,1} \\ \vdots \\ w_{33,1} \end{bmatrix} u_1(t) + \begin{bmatrix} w_{1,2} \\ w_{2,2} \\ \vdots \\ w_{33,2} \end{bmatrix} u_2(t) + \cdots + \begin{bmatrix} w_{1,33} \\ w_{2,33} \\ \vdots \\ w_{33,33} \end{bmatrix} u_{33}(t). \quad (11)$$

